The transcription factor IRF4 is essential for T cell receptor affinity mediated metabolic programming and clonal expansion of T cells

Kevin Man[1,2], Maria Miasari[1,2], Wei Shi[1,3], Annie Xin[1,2], Darren C. Henstridge[5], Simon Preston[1,2], Marc Pellegrini[1,2], Gabrielle T. Belz[1,2], Gordon K. Smyth[1,4], Mark A. Febbraio[5], Stephen L. Nutt[1,2], Axel Kallies[1,2]

[1] The Walter and Eliza Hall Institute of Medical Research, 1G Royal Parade, Parkville, Victoria, 3050, Australia.

[2] The Department of Medical Biology, University of Melbourne, Parkville, Victoria, 3010, Australia.

[3] The Department of Computing and Information Systems, University of Melbourne, Parkville, Victoria, 3010, Australia.

[4] The Department of Mathematics and Statistics, University of Melbourne, Parkville, Victoria, 3010, Australia.

[5] Cellular and Molecular Metabolism Laboratory, Baker IDI Heart and Diabetes Institute, Melbourne, Victoria, 3004, Australia.

Correspondence should be addressed to A.K. (kallies@wehi.edu.au).

Key words. IRF4, T cell receptor, affinity, transcription, $CD8^+$, differentiation, metabolic function, glycolysis

Abstract. During immune responses T cells are subject to clonal competition, which leads to the predominant expansion of high-affinity clones; however, there is little understanding how this process is controlled. We demonstrate that transcription factor IRF4 is induced in a T cell receptor (TCR) affinity-dependent manner and functions as a dose-dependent regulator of the metabolic function of activated T cells. IRF4 regulates the expression of key molecules required for aerobic glycolysis of effector T cells, and is essential for clonal expansion and maintenance of effector function of antigen-specific $CD8^+$ T cells. Thus, IRF4 is an indispensable molecular rheostat that translates TCR affinity into appropriate transcriptional programs linking metabolic function with clonal selection and effector differentiation of T cells.

T cell responses are guided by multiple cell extrinsic cues, including antigen, co-stimulatory molecules and cytokines, which lead to the induction of transcriptional regulators that ultimately control the differentiation of activated T cells into effector and memory T cells. Several critical transcriptional regulators and some of their down-stream targets involved in this process have been identified[1,2]. The best-known transcription factors that control $CD8^+$ T cell differentiation in the periphery are the T-box transcription factors T-bet and Eomes, which act in concert during the differentiation of effector and memory T cells[3]. In addition the transcription factor Blimp1 was found to drive terminal differentiation of short-lived cytotoxic effector T cells at the expense of memory T cells[4,5], and the opposing activities of inhibitor of DNA binding (Id)2 and Id3, which antagonize the DNA binding activity of E-proteins, were revealed[6,7].

The interaction between antigen and its cognate T cell receptor (TCR) is a critical determinant of the outcome of T cell responses[8]. While the early phase of T cell responses is characterized by the expansion of a diverse array of antigen-specific clones with a broad range of affinities for the antigen-derived peptide epitopes, the later phase is dominated by a limited number of clones, in particular those with higher affinities. This 'focussing' of the T cell response is the result of clonal competition and leads to the establishment of dominant epitope-specific T cell clones of high affinity[9-13] that are critical for the control of pathogens[14-16]. Recruitment, proliferation and acquisition of effector function are comparable between $CD8^+$ T cells responding to a high or low affinity antigen, respectively[17]. However, T cells responding to a low-affinity antigen fail to accumulate during infection, thus contribute only minimally to the effector population at the peak of the response[17]. Differential migration and survival[17-19] or 'diversion' into memory[20-22] were linked to the diminished expansion of low-affinity stimulated $CD8^+$ T cells. Thus, differences in clonal expansion of T cells are the consequence of multiple effects including proliferation and cell death. It was, however, unclear how TCR signals resulting from interactions with ligands of various affinities could be translated into distinct transcriptional programs and differentiation outcomes.

The transcription factor IRF4 has been shown to be required for multiple functions in the immune system[23] including plasma cell differentiation[24,25], regulatory T (T_{reg}) cell function[26,27] and for the development of several $CD4^+$ T cell helper (Th) subsets[28-30]. Its role in the differentiation and function of cytotoxic effector T cells, however, has not been examined in any detail. We show here that *Irf4*-deficient mice fail to mount a productive $CD8^+$ T cell response during viral or bacterial challenge and demonstrate that IRF4 is required for ongoing expansion of antigen-specific $CD8^+$ T cell clones and for the maintenance of effector functions. We establish that IRF4 expression is strictly controlled by TCR affinity, and that IRF4 acts in a dose dependent manner to promote the preferential expansion of high affinity T cell clones. Finally, we reveal that IRF4 is a key regulator of metabolic function of effector $CD8^+$ T cells whose graded expression determines the level of aerobic glycolysis after T cell activation. Thereby, our data lead to a model in which IRF4 occupies the centre of a transcriptional network, which controls metabolic programming and underlies affinity selection, clonal competition and maintenance of effector function of $CD8^+$ T cells during an immune response.

Results

IRF4 is essential for a productive CD8$^+$ T cell response

IRF4 is required for the cytotoxic response during infection of mice with Lymphocytic choriomeningitis virus (LCMV)[23]. However, it was unclear whether this was due to diminished effector functions, failed differentiation or reduced numbers of antigen-specific CD8$^+$ T cells in the absence of IRF4. To examine in detail the roles of IRF4 in CD8$^+$ T cells responding to a pathogen we intranasally infected IRF4-deficient (*Irf4*$^{-/-}$) and wildtype control mice with influenza virus (strain HKx31). Ten days later at the peak of the response we examined CD8$^+$ T cells specific for the two dominant epitopes (NP_{366} and PA_{224}) using tetrameric complexes. While we detected antigen-specific CD8$^+$ T cells at the expected frequencies in wildtypes, such cells were almost undetectable in *Irf4*$^{-/-}$ mice (**Fig. 1a**). This was true for all organs examined, including the spleen, the lung-draining mediastinal lymph node and the lung itself (**Fig. 1a, Supplementary Fig. 1a**). Similarly, expression of KLRG1, a marker for short-lived effector cells, was not detectable on IRF4-deficient CD8$^+$ T cells (**Fig. 1a**), and restimulation of these cells did not result in detectable interferon-γ (IFN-γ) secretion or granzyme B (GzmB) expression (**Fig. 1b**).

As IRF4 is expressed in various lymphoid and non-lymphoid cells and has multiple critical functions in the immune system, it was possible that the lack of a CD8$^+$ T cell response in *Irf4*-deficient mice was due to CD8$^+$ T cell extrinsic defects. To address this question, we generated mixed bone marrow chimeric mice containing congenically marked wildtype cells (Ly5.1) and *Irf4*-deficient (Ly5.2) cells. These mice showed normal development of wildtype and *Irf4*$^{-/-}$ T cells in the thymus and the spleen, and similar to their wildtype counterparts *Irf4*$^{-/-}$ CD8$^+$ T cells were largely of a naive phenotype (**Supplementary Fig. 1b**). Infection of these chimeric mice with influenza virus with or without prior priming with a heterologous influenza virus strain (PR8) resulted in a robust CD8$^+$ T cell response in the wildtype but not in the *Irf4*-deficient compartment, clearly indicating a CD8$^+$ T cell intrinsic requirement for IRF4 (**Fig. 1c-f, Supplementary Fig. 2c-f**).

To assess whether the defective CD8$^+$ T cell response observed in the absence of IRF4 also occurred in a systemic infection model, we challenged mixed bone marrow

chimeric mice intravenously with LCMV. Analysis of these mice revealed a strong activation and effector T cell differentiation of large proportions of wildtype $CD8^+$ T cells as measured by downregulation of the adhesion molecule L-selectin (CD62L) and upregulation of KLRG1, which was largely abolished in the absence of IRF4 (**Fig. 1g**). Similarly and consistent with the data obtained in the influenza model we detected very few antigen-specific $CD8^+$ T cells in the *Irf4*-deficient compartment of LCMV infected chimeric mice (**Fig. 1h, Supplementary Fig. 2g-h**).

To test the impact of IRF4 deletion after activation, we made use of a floxed allele of *Irf4*, which was bred to a transgenic mouse strain expressing Cre recombinase under the control of *GzmB* gene regulatory elements[31]. Deletion of the *Irf4* allele occurred upon induction of *GzmB*, i.e. after T cell activation, and was marked by expression of green fluorescent protein (GFP)[24] (**Supplementary Fig. 2a**). In line with our previous results, infection with LCMV revealed a strong reduction of antigen-specific cells in the $CD8^+$ T cell population that had deleted *Irf4* (**Supplementary Fig. 2b, c**). The few remaining *Irf4*-deficient antigen-specific $CD8^+$ T cells showed a marked loss of $KLRG1^+IL\text{-}7R^-$ short-lived effector cells, and an increased proportion of $CD62L^+$ cells. These cells also showed an overall reduction of IL-7R expression, even in the $KLRG1^-$ fraction (**Supplementary Fig. 2d, e**). In summary, these data demonstrate that IRF4 is required for a productive $CD8^+$ T cell response in a cell-intrinsic manner.

IRF4 is required for the survival of activated T cells

To examine the expression pattern of IRF4 in $CD8^+$ T cells during activation, we cultured naive $CD8^+$ T cells with anti-CD3 and anti-CD28 antibodies *in vitro*. IRF4 was not expressed in naive T cells, but was rapidly induced following stimulation and remained expressed at high levels for the time points examined (**Fig. 2a, upper panel**). Subsequent culture of stimulated $CD8^+$ T cells in cytokines in the absence of TCR stimulation resulted in down-regulation of IRF4 (**Fig. 2a, lower panel**). Thus, IRF4 is induced by TCR signalling and high expression of IRF4 requires ongoing stimulation.

We then examined T cell activation in the absence of IRF4 *in vitro*. Expression of early activation and memory markers such as CD69, CD25, CD62L and CD44 was

comparable in wildtype and *Irf4*-deficient $CD8^+$ T cells, indicating that early activation events were not impaired by *Irf4*-deficiency (**Fig. 2b; Supplementary Fig. 3a**). Proliferation of *Irf4*$^{-/-}$ $CD8^+$ T cells as measured by the dilution of the cell division tracker CTV was unchanged, as was expression of the effector molecules IFN-γ, GzmB and T-bet (**Fig. 2c, d; Supplementary Fig. 3b**). Thus, IRF4 was not required for activation, proliferation or early effector differentiation of $CD8^+$ T cells *in vitro*. Further analysis of the T cell cultures, however, revealed that *Irf4*$^{-/-}$ $CD8^+$ T cells did not expand to the same numbers as wildtype cells (**Fig. 2e**), suggesting increased cell death. Consistent with this possibility a larger fraction of *Irf4*-deficient $CD8^+$ T cells showed Annexin V staining and more IRF4-deficient $CD8^+$ T cells expressed the active form of Caspase 3, two hallmarks of apoptosis (**Fig. 2f**). To test if programmed cell death was the cause for the reduced $CD8^+$ T cell numbers in the absence of IRF4, we crossed *Irf4*$^{-/-}$ mice onto transgenic mice that overexpress the pro-survival molecule Bcl-2 in all hematopoietic cells (Vav-Bcl2tg)[32] or to mice deficient in the pro-apoptotic molecule Bim[33]. However, neither combination could restore the antigen-specific $CD8^+$ T cell compartment in the absence of IRF4 (**Supplementary Fig. 3c, d**), indicating that deregulation of the intrinsic death pathway is not the primary cause for the diminished cell survival in the absence of IRF4.

IRF4 is required for ongoing T cell expansion and effector function

In order to examine T cell expansion and effector differentiation *in vivo* in more detail, we generated *Irf4*-deficient TCR-transgenic mice (*Irf4*$^{-/-}$ OT-I), in which $CD8^+$ T cells are specific for a peptide epitope of the model antigen ovalbumin (OVA)[34]. We co-transferred equal numbers of congenically marked *Irf4*$^{-/-}$ (Ly5.2) and *Irf4*$^{+/+}$ (Ly5.1) OT-I T cells into F1 (Ly5.1 x Ly5.2) recipient mice, which were infected with an influenza virus that expressed OVA[35]. This allowed us to track T cell activation, expansion and acquisition of effector function in a competitive situation with both cell populations in a wildtype environment. Examination of the donor T cells early after cell transfer indicated that neither recruitment, phenotype, nor initial expansion of the $CD8^+$ T cells depended on IRF4 (**Fig. 3a-c, Supplementary Fig. 4a**). Over the course

of the immune response, however, *Irf4*$^{-/-}$ OT-I T cells were grossly outcompeted by their wildtype counterparts in all organs examined (**Fig. 3b, c**) with the most pronounced cell loss occurring in the lungs (**Supplementary Fig. 4b**). Expression of effector molecules such as IL-2, IFN-γ, TNF and GzmB could be observed in both populations early during infection; however, *Irf4*-deficient cells progressively lost their effector functions (**Fig. 3d, Supplementary Fig. 4c**) and showed strongly increased surface expression of CD62L (**Fig. 3e**). Similar to our *in vitro* data, proliferation was similar up to day 3, but was markedly impaired by day 5 (**Supplementary Fig. 4d**). When we performed the above-described experiments with *Irf4*$^{+/-}$ CD8^{+} T cells, we observed a pronounced effect of IRF4 dosage on expansion and phenotype of the cells (**Fig. 3f, Supplementary Fig. 4e-h**). In summary, these data indicate that IRF4 is dispensable for early events of CD8^{+} T cell activation and differentiation but is required for the maintenance of expansion and effector function in a dose dependent manner.

Induction of IRF4 is T cell receptor affinity dependent

As TCR stimulation induced IRF4 expression, which was essential for efficient T cell expansion, we reasoned that IRF4 might be involved in translating TCR affinity signals into appropriate CD8^{+} T cell expansion and differentiation. To test this hypothesis, we used OVA peptide variants of different affinities for the OT-I T cell receptor, including the high affinity wildtype peptide SIINFEKL (N4), and the peptides Q4 and V4 that bind with intermediate and low affinity, respectively[36]. *In vitro* stimulation of OT-I T cells with wildtype OVA-peptide (N4) induced high amounts of IRF4 protein. In contrast, the altered affinity peptide variants induced intermediate (Q4) or low (V4) amounts of IRF4 protein, indicating that IRF4 expression depends on the affinity of antigen-TCR interactions (**Fig. 4a**).

To validate these findings *in vivo*, we inoculated naive congenically marked recipient mice with recombinant *Listeria monocytogenes* expressing N4, Q4 or V4 OVA peptide variants[17] and subsequently transferred wildtype OT-I T cells into these mice. After infection with *Listeria*-N4, IRF4 expression was heterogeneous early during the

T cell response; however, the majority of OT-I T cells were homogenously high for IRF4 by day 5 post infection (**Fig. 4b**). Analysis of CTV labelled OT-I T cells transferred into *Listeria*-N4 infected mice showed that OT-I T cells expressing high amounts of IRF4 protein ($IRF4^{hi}$) underwent much more pronounced proliferation than those with low amounts of ($IRF4^{lo}$) (**Fig. 4c**) consistent with the idea that IRF4 drives expansion of $CD8^+$ T cells. IRF4 expression in OT-I T cells in mice infected with *Listeria*-Q4 or V4 was much lower, confirming that affinity signals control the level of IRF4 expression *in vivo* (**Fig. 4d**).

To test if loss of or lower amounts of IRF4 had an impact on $CD8^+$ T cells responding to antigens of different affinity we co-transferred equal numbers of congenically marked IRF4-deficient ($Irf4^{-/-}$) or IRF4-haploinsuffcient ($Irf4^{+/-}$) OT-I T cells together with wildtype ($Irf4^{+/+}$) OT-I T cells into recipient mice and infected them with *Listeria*-N4 and *Listeria*-V4, respectively. Similar to the data obtained in the influenza model, initial proliferation was comparable between $Irf4^{-/-}$ and wildtype OT-I T cells as assessed by CTV dilution (**Fig. 4e**); however, $Irf4^{-/-}$ OT-I T cells showed severely impaired expansion in comparison to wildtype OT-I T cells, and even $Irf4^{+/-}$ OT-I T cells were outcompeted by wildtype OT-I T cells (**Fig. 4f, Supplementary Fig. 5a**). Early after infection, $Irf4^{-/-}$ and wildtype OT-I T cells were present in similar numbers in the spleens and showed an even somewhat elevated representation in lymph nodes (**Supplementary Fig. 5b**), suggesting that differential access to antigen and lymphoid structures was not responsible for the gross under-representation of IRF4-deficient cells at later time points. We did, however, detect a smaller proportion of $Irf4^{-/-}$ OT-I T cells in the liver, suggesting that IRF4 impacts on the ability of $CD8^+$ T cells to migrate to non-lymphoid tissues (**Supplementary Fig. 5b**). In line with our data from mice with a conditional deletion of *Irf4*, IRF4-deficient OT-I T cells showed strongly reduced KLRG1 expression indicating impaired differentiation of short-lived effector cells (**Fig. 4g**).

As expected, expansion of wildtype OT-I T cells was strongly enhanced in the high affinity infection model. In contrast, high affinity signals did not result in increased numbers of *Irf4*-deficient cells (**Fig. 4h, Supplementary Fig. 5c**). Similar results were obtained when isolated OT-I T cells were stimulated *in vitro* with peptides of different affinity (**Fig. 4i, Supplementary Fig. 5d**). These data indicate that IRF4 is

required for the 'translation' of affinity signals from the TCR into appropriate T cell expansion.

IRF4 drives most TCR-affinity dependent transcriptional changes

To identify the transcriptional program regulated by IRF4 during TCR affinity-driven expansion of $CD8^+$ T cells, we performed RNA-sequencing analysis on wildtype or IRF4-deficient OT-I T cells stimulated with either high or low affinity OVA peptides. 683 genes showed statistically significant differential expression (>2 fold; false discovery rate <0.05) between wildtype cells stimulated with high (N4) or low affinity (V4) peptides, respectively (**Fig. 5a, b**). In contrast, a comparison between *Irf4*$^{-/-}$ cells stimulated with N4 versus V4 peptide recovered only 45 genes that were differentially expressed, indicating that the majority of TCR affinity driven transcriptional changes in $CD8^+$ T cells depend on IRF4 (**Fig. 5a, b, Supplementary Table S1**). This was confirmed by the finding that most genes (73.8%) that were differentially expressed between high and low affinity peptide stimulated wildtype OT-I T cells (affinity-driven DE genes) were also found to be differentially expressed between *Irf4*$^{-/-}$ and *Irf4*$^{+/+}$ OT-I T cells stimulated with high affinity N4 (IRF4-driven DE genes) (**Fig. 5b**). A Pearson's correlation analysis between these two data sets revealed a strong correlation in the directional expression changes, which was lost when this analysis was performed on *Irf4*-deficient cells (**Fig. 5c**).

As expected, known targets of IRF4, including *Prdm1* (encoding Blimp1), and other key-regulators involved in $CD8^+$ T cell differentiation and function, such as *Eomes*, *Runx3*, *Tcf7*, *Il7r*[1,2,37] (**Fig. 5d-e**) were amongst the differentially expressed genes, for some of which differential expression was confirmed on a protein level (**Supplementary Fig. 5e-h**). Ingenuity Pathway Analysis identified 'Carbohydrate Metabolism, Molecular Transport, Small Molecule Biochemistry' as the functional molecular network most significantly associated with transcripts differentially expressed between wildtype and *Irf4*-deficient $CD8^+$ T cells (P=0.0002, **Supplementary Fig. 6a**), and key regulators of cellular metabolism including *Foxo1, Foxo3* and *Hif1a*[38-40] were found to be significantly reduced in their mRNA expression (**Fig. 5f**). Thus, the TCR-affinity dependent transcriptional program of

$CD8^+$ T cells includes key-regulators of T cell differentiation and cellular metabolism and requires IRF4.

IRF4 binds genes required for key metabolic functions

To identify direct transcriptional targets of IRF4 in $CD8^+$ T cells during activation and expansion we performed genome wide chromatin immuno-precipitation (ChIP) sequencing using IRF4-specific antibodies. Analysis yielded 3338 IRF4 binding sites (P value $<10^{-5}$), 91% of which could be mapped to a total of 2268 known genes. Of these binding sites 36% (1095) were found in the 20kb upstream of the transcriptional start site, 56% (1716) in gene bodies and 8% (227) in the 5kb downstream of the transcriptional end site. 470 (75%) of the differentially expressed genes (N4, *Irf4*$^{-/-}$ versus *Irf4*$^{+/+}$) to which IRF4 binding sites were assigned showed significantly downregulated expression (>2 fold; false discovery rate <0.05), suggesting that IRF4 acts largely as a transcriptional activator in $CD8^+$ T cells.

De-novo binding motif analysis of the high confidence sites revealed a strong enrichment for AP1 binding sites, with many conforming to the recently described IRF4-AP1 composite DNA binding site (AICE) motifs, IRF4-AP1 or IRF4-NNNN-AP1[41-43] (**Fig. 6a, b**). Genes directly bound by IRF4 included known IRF4 targets, such as *Prdm1*, *Il10*, *Il23r* and *Ctla4*[27,41,43], as well as other genes with critical functions in $CD8^+$ T cells, including *Runx3*, *Tcf-7*, *Ccr7* and *Il7r* (**Fig. 6c, and data not shown**). Importantly, two transcription factors that regulate T cell quiescence and glycolytic metabolism following antigen exposure, *Foxo1* and *Hif1a*, were directly bound by IRF4 (**Fig. 6d**), supporting a central role for IRF4 in integrating downstream factors that regulate differentiation and metabolic programming in T cells.

IRF4 is required for metabolic function of CD8$^+$ T cells

Activation of T cells induces a dramatic rewiring of metabolic processes as cells shift from oxidative phosphorylation (OXPHOS) to aerobic glucolysis to fulfil the bioenergetic and biosynthetic demands of rapid proliferation and differentiation[44-47]. To examine if IRF4 plays a role in cellular metabolism we measured mitochondrial membrane potential by MitoTracker staining. Mitochondrial membrane potential was intact or even elevated up to 24 hours post activation, but decreased at 48 hours in the absence of IRF4 (**Fig. 6e**). To study the function of IRF4 in more detail, we measured the bioenergetic profiles of naive as well as activated wildtype and *Irf4*-deficient CD8$^+$ T cells using extracellular flux assays. As expected, the oxygen consumption rate (OCR) was strongly induced upon activation of control CD8$^+$ T cells (**Fig. 6f**) In contrast, *Irf4*-deficient CD8$^+$ T cells, while initially increasing OCR relative to naive T cells, were not able to further induce OCR 48 h after activation (**Fig. 6f**). Similarly, ATP production, measured in response to the ATP synthase inhibitor oligomycin, and maximal respiratory capacity, determined by treatment with the electron transport chain uncoupler FCCP, were impaired in the absence of IRF4 (**Fig. 6g, Supplementary Fig. 6b, c**).

In addition to the reduced OCR, we found that the glycolytic capacity of activated *Irf4*-deficient T cells, as measured by the extracellular acidification rate (ECAR), was strongly reduced (**Fig. 6h, Supplementary Fig. 6d, e**). In line with this result, *Irf4*-deficient T cells demonstrated reduced uptake of a fluorescently labelled glucose analogue (2NB-DG) at 24 h (**Fig. 6i**), and produced significantly less extracellular L-lactate compared to wildtype cells at 48 h after activation (**Fig. 7a**). As expected the OCR/ECAR ratio dropped dramatically in wildtype cells as they switched from OXPHOS to aerobic glycolysis during activation; however, this was markedly impaired in *Irf4*-deficient cells (**Fig. 7b**). In line with their reduced glycolytic capacity *Irf4*-deficient T cells, in addition to *Hif1a,* showed reduced expression of several genes encoding key regulators of glycolysis including glucose transporters Glut1 and Glut3 (*Slc2a1* and *Slc2a3*), hexokinase 2 (*Hk2*) and 6-phosphofructo-2-kinase/fructose-2,6-biphosphatase 3 (*Pfkfb3*), aldolases (*Aldoa*, *Aldoc, Aldoart1*)[48] as well as other genes required for metabolic function of proliferating T cells, some of which were direct targets of IRF4 (**Fig. 7c, d, Supplementary Fig. 7a**). Most of the genes regulated by IRF4 were induced during CD8$^+$ T cell activation whereas genes

that were constitutively expressed (such as *Hk1* or *Gapdh*) were not impacted on by the loss of IRF4 (**Supplementary Fig. 7a, b, and data not shown**). Quantitative RT-PCR analysis confirmed that expression of key regulators of glycolysis but not OXPHOS required IRF4 for their transcription early after activation and subsequently for their sustained expression during proliferation (**Fig. 7e**). In line with the finding that T cells in the absence of available glucose can sustain proliferation at least partially through OXPHOS[49], we observed that a large number of genes involved in this process were upregulated in the absence of IRF4 (**Supplementary Fig. 7c**). However, the vast majority of these genes did not show binding of IRF4, suggesting that this upregulation was a compensatory mechanism in response to the reduced glycolytic capacity of T cells in the absence of IRF4. In line with their ability to undergo blastogenesis and to induce early glycolysis, we found that the transcription factor Myc, which induces metabolic reprogramming in activated T cells[48], was expressed at comparable levels in wildtype and *Irf4*-deficient T cells (**Fig. 7f**). IPA identified Myc as the "Top Upstream Regulator" (p value of overlap $4.57x10^{-18}$) suggesting that many of the Myc regulated genes are also regulated by IRF4. Thus, although IRF4 was not required for the initial activation-induced metabolic switch from fatty acid oxidation to glycolysis it was essential for high-level glycolytic turnover and for sustained mitochondrial activity in activated T cells.

IRF4 links TCR affinity, metabolism and migration of CD8 T cells

To test if impaired metabolic function may be responsible for the aborted clonal expansion of IRF4-deficient T cells we performed a series of metabolic tests on OT-I T cells responding to *Listeria*-OVA early during infection. IRF4-deficient OT-I T cells isolated from *Listeria*-OVA (N4) infected mice exhibited significantly impaired oxygen consumption and glucose turnover as measured by ECAR (**Fig. 8a**), as well as diminished response to glucose challenge (**Fig. 8b**). Similar to our *in vitro* results we also observed an increased OCR/ECAR ratio as well as a reduced rate of 2NB-DG uptake and lactate production in the IRF4-deficient OT-I T cells (**Fig. 8c-e**). In line with their reduced metabolic activity, responding *Irf4*$^{-/-}$ OT-I T cells were significantly smaller than their wildtype counterparts and showed reduced expression of the transferrin receptor CD71 (**Fig. 8f, g**). In keeping with our finding that low affinity TCR ligands induce little IRF4 protein expression (**Fig. 4d**), the reduced

metabolic rates, cell size and CD71 expression in the absence of IRF4 were strikingly similar to wildtype OT-I T cells responding to *Listeria* expressing the low affinity OVA-V4 (**Fig. 8d-g**).

Metabolic function of T cells as well as affinity driven signals critically control $CD8^+$ T cell homing and migration[38,45]. We thus hypothesised that IRF4 may be involved in linking these two pathways. Consistent with this idea, we found that the reduction of *Irf4*-deficient cells during influenza and *Listeria* infection was most pronounced in non-lymphoid organs such as lung and liver (**Supplementary Fig. 4b, 5b**), suggesting that IRF4 is required for correct tissue localization of T cell responding to antigen. In summary these data indicate that IRF4 is required for the metabolic programming and for the change of migratory capacities of $CD8^+$ T cells after activation in a TCR affinity dependent manner.

IRF4 is limiting for low-affinity $CD8^+$ T cell responses

Overall our data suggested that IRF4 expression is a critical and limiting factor in the expansion of $CD8^+$ T cells and that low expression of IRF4 is responsible for the loss of low-affinity $CD8^+$ T cells from ongoing immune responses. To directly test this model we retrovirally over-expressed IRF4 along with a GFP reporter gene in wildtype OT-I T cells. These cells or cells transduced with a control virus were then adoptively transferred into congenically marked recipient mice, which were subsequently infected with *Listeria*-V4. OT-I T cells overexpressing IRF4 expanded significantly better (**Fig. 8h**), directly demonstrating that IRF4 expression is the limiting factor during a low-affinity T cells response.

Discussion

IRF4 is critically involved in the differentiation multiple lymphocyte lineages and T cell subsets. Its coordinated activity and interaction with lineage-specific transcription factors is exemplified in a recently described network of transcription factors required for Th17 differentiation[42]. We have here identified a new IRF4-dependent transcriptional network in $CD8^+$ T cells that is driven by TCR affinity and required for the transcriptional regulation of the metabolic program operating during clonal

expansion of antigen-activated T cells. Due to a tight requirement for IRF4, low-affinity stimulated T cells that express limited amounts of IRF4 or T cells that lack IRF4 show dramatically diminished antigen-specific responses and exhibit impaired effector differentiation and function.

Effector and memory $CD8^+$ T cell differentiation is controlled by the coordinated and dynamic expression of a series of transcriptional regulators, including T-bet, Blimp1, Runx3, Eomes, Bcl6, Tcf-1, Id2, and Id3[1,2,37]. Our data reveal IRF4 as another central transcriptional regulator of antigen-stimulated $CD8^+$ T cells that is essential for a productive $CD8^+$ T cell response. During an immune response antigen-specific *Irf4*-deficient $CD8^+$ T cells rapidly lose effector function and undergo aborted clonal expansion. While this can be largely attributed to a failure of metabolic function, as discussed below, dysregulation of several transcription factors required for the coordinate development of effector and memory T cells may also contribute. Similar to T_{reg} cells[27] IRF4 in $CD8^+$ T cells is directly required for the induction of *Prdm1* (encoding Blimp1). IRF4-deficient $CD8^+$ T cells also show diminished expression of *Runx3* and *Tcf-7* (encoding Tcf-1), both of which we identify here as direct target genes of IRF4. Conversely, IRF4-deficient antigen-specific $CD8^+$ T cells display higher amounts of Eomes, but there was no evidence for direct binding of IRF4 to the *Eomes* gene locus. As the balance between Blimp1 and T-bet on one side and Eomes on the other side is critical for differentiation of cytotoxic effector versus memory T cells[1,2], IRF4 appears to promote effector differentiation at the expense of memory development. Our data suggest that during the clearance of an infection, IRF4 expression diminishes along with the reduced antigenic load thus allowing the upregulation of Eomes and the development of memory cells.

T cell activation induces a tightly controlled metabolic shift from OXPHOS to aerobic glycolysis to provide energy required for rapid proliferation, differentiation and effector function[44-47]. Our experiments demonstrate that IRF4 is a central regulator of this process. It is required for the expression of transcription factors, including Hif1a and Foxo1, that are essential for the metabolic functions of T cells[38-40] and controls expression of genes encoding rate-limiting components of the glycolytic pathway including glucose transporters and enzymes involved in glycolysis, which are induced during normal T cell activation (**Supplementary Fig. 7**). Although IRF4 was

dispensable for the initial induction of aerobic glycolysis, it was essential at later time points for high levels of glycolytic turnover, resulting in a marked increase in the OCR/ECAR ratio in *Irf4*$^{-/-}$ cells, suggesting that antigen-activated IRF4-deficient T cell depend on oxidative phosphorylation rather than glycolysis. Interestingly, IRF4-deficient cells initially maintained proliferation but rapidly lost effector function, which is in line with a recent report indicating that OXPHOS is sufficient to at least partially sustain proliferation but not effector function[49]. IRF4-deficient T cells not only showed a pronounced defect in glycolysis but also displayed severely diminished mitochondrial function, in particular at later time points after activation. Our experiments, however, provided little evidence for a direct role for IRF4 in regulating genes involved in OXPHOS (**Fig. 7e**). Since reduced glycolysis preceded the reduction of oxygen consumption in *Irf4*$^{-/-}$ cells, we propose that reduction in glycolysis is responsible for the diminished OCR. The observed defects in OXPHOS, however, may also be due to deregulation of redox state and increased oxidative stress, which could be contributed to by decreases in expression of Foxo1 and Foxo3[50]. Overall, *Irf4*$^{-/-}$ T cells fail to efficiently metabolize glucose and show impaired OXPHOS, but it is currently unclear whether failure of glycolysis or mitochondrial function or both are the ultimate cause of the aborted clonal expansion in the absence of IRF4.

Myc has been identified as a key regulator during the induction of aerobic glycolysis[48]. Importantly, *Irf4*-deficient T cells were able to induce Myc upon activation and to undergo normal blastogenesis, supporting the view that Myc is a main driver of the early metabolic switch that occurs upon activation. In line with recent reports that showed that the activity of IRF4 in requires coordinated binding with AP1 transcription factors to an AP1-IRF4 composite motif (AICE)[41-43], most IRF4 binding sites revealed by our ChIP sequencing experiments in CD8^{+} T cells were AP1-IRF4 composite sites. These data suggest that IRF4, AP1 and Myc act in concert to regulate metabolic programming of T cells upon activation and may be part of a conserved transcriptional program that acts in all activated T cells.

The process of clonal selection and competition during an immune response results in increased overall affinity of the antigen-specific T cell population[9-13] and is of fundamental importance for pathogen control[14-16]. While several mechanisms have

been proposed to explain this observation[17-22], the molecular foundation for this phenomenon was poorly understood. We show here, that TCR affinity regulates the magnitude of IRF4 expression and demonstrate that IRF4 acts in a dose dependent manner to control the expression of the majority of TCR-affinity regulated genes, most notably genes involved in cellular metabolism. IRF4 can therefore operate as a molecular link between TCR affinity and an appropriate T cell response, including expansion and effector differentiation. These results in conjunction with our observation that low-affinity T cells show diminished uptake of glucose strongly suggest that IRF4 regulates clonal expansion of T cells by maintaining metabolic activity in a TCR affinity dependent manner. Our data indicate that only antigen-specific T cells bearing TCR's of sufficient affinity to their cognate peptide-antigen induce high IRF4 expression. Thereby, they can efficiently switch to aerobic glycolysis, sustain high metabolic activity and thus maintain ongoing clonal expansion and effector differentiation. In contrast, clones of lower affinity, which express diminished amounts of IRF4, will be selectively lost or diverted into early memory development during the course of the immune response. The result of such a process is a 'focussed' antigen-specific T cell population that at the peak of the response is dominated by a small number of high-affinity T cell clones (**Supplementary Fig. 8**). Thus, our data identify IRF4 as the central molecular rheostat in a transcriptional network that links metabolic function to clonal expansion and effector differentiation and provides a molecular framework for the clonal selection and competition of T cells during an immune response.

Database accession numbers

Acknowledgments. We wish to thank Tak Mak, Ulf Klein, Susan Kaech, Philippe Bouillet and Suzanne Cory for mice, Dietmar Zehn for *Listeria*-OVA variants, Andrew Lew for HKx31-OVA influenza virus, and Shoukat Sterle, Rebecca Cole, Nadia Iannarella and Liana Mackiewicz for expert technical support. We express our gratitude to David Segal, Clovis Palmer, Phil Hodgkin, Lynn Corcoran, Susanne Heinzel and Frederick Masson for reagents and helpful discussion. This work was supported by grants and fellowships from the National Health and Medical Research Council of Australia (MP, GTB, GKS, SLN, MAF, AK), the Sylvia and Charles Viertel Foundation (AK, GTB) and Howard Hughes Medical Institute (GTB), the

Australian Research Council (SLN, AK), the National Heart Foundation (DCH) and the WEHI Genomics Fund (AK, GB, WS), the Victorian State Government Operational Infrastructure Support and Australian Government NHMRC Independent Research Institute Infrastructure Support scheme.

Figure legends

Figure 1 IRF4 is essential for a productive CD8$^+$ T cell response. (**a)** Wildtype (*Irf4*$^{+/+}$) or *Irf4*-deficient (*Irf4*$^{-/-}$) mice were infected with influenza virus (strain HKx31). 10 days later splenic CD8$^+$ T cells were analysed by flow cytometry for the presence of antigen-specific cells by tetramer staining or effector T cells using an anti-KLRG1 antibody (left panel). Frequencies of CD8$^+$ T cells specific for two epitopes (NP_{366} and PA_{224}) (right panel) in the spleen. (**b)** CD8$^+$ T cells as in (a) were restimulated with NP_{366} peptide and analysed for effector molecule expression. (**c-e)** Analysis of antigen-specific CD8$^+$ T cells in chimeric mice generated by reconstituting lethally irradiated Ly5.1 mice with *Irf4*$^{-/-}$ or wildtype (both Ly5.2) bone marrow mixed with Ly5.1 bone marrow as indicated. Chimeric mice were infected with influenza virus (HKx31) without prior priming (c) or 6 weeks after priming with a heterologous influenza virus (strain PR8, d-f). (**e)** Frequencies of NP_{366} specific CD8$^+$ T cells in the spleen. **f.** CD8$^+$ T cells as in (d) were restimulated with NP_{366} peptide and analysed for effector molecule expression. (**g-h)** Chimeric mice as in (c) were infected with LCMV. Frequencies of effector CD8$^+$ T cells were measured by staining for KLRG1$^+$ or CD62L$^-$ cells (g) or by tetramer detection of CD8$^+$ T cells specific for the LCMV epitopes GP_{33} or NP_{396} in the spleen (h). Flow cytometry is representative for 2-3 individual experiments containing 2-3 mice per group. Data points in graphs represent cell frequencies in individual mice as indicated (* $P<0.0001$, NS - not significant). Horizontal line shows the mean ±S.E.M.

Figure 2 IRF4 in CD8$^+$ T cells is not required for activation, proliferation and effector molecule expression but for prevention of cell death. (**a)** MACS-sorted CD62L$^+$CD8$^+$ T cells (upper panel) or naive flow-sorted CD44$^-$CD62L$^+$ CD8$^+$ T cells (lower panel) of the indicated genotypes were cultured in the presence of anti-CD3 and CD28 antibodies and IL-2. Protein extracts were prepared at the indicated times. Some cells were re-cultured for further expansion in medium containing IL-2 or IL-15

alone for 2 days (lower panel). (**b)** Expression of activation markers on $CD8^+$ T cells as in (a) after 40 h in culture. (**c)** Naive $CD8^+$ T cells of the indicated genotypes were flow-sorted, labelled with cell division tracker dye CTV, cultured as in (a), and analysed at times as indicated. (**d)** Intracellular staining of effector molecules of $CD8^+$ T cells as in (c) after 4 days in culture. (**e)** Mean numbers of live $CD8^+$ T cells ± S.D. cultured on plates coated with anti-CD28 and varying concentrations of anti-CD3 antibody as indicated (* $P<0.0001$, 2-way ANOVA). (**f)** Staining of Annexin V and intracellular Caspase 3 (Casp 3) of cells cultured for 3 days as in (a). Experiments in a-f are representative of 3-5 independent experiments, b-e each performed in triplicates.

Figure 3 IRF4 is dispensable for early T cell proliferation and effector molecule expression *in vivo* but required for ongoing clonal expansion and maintenance of effector function in a dose-dependent manner. $2.5x10^5$ $CD8^+$ T cells isolated from OT-I TCR transgenic mice either on a wildtype (Ly5.1) or IRF4-deficient (*Irf4*$^{-/-}$) and haploinsufficient (*Irf4*$^{+/-}$) (both Ly5.2) background as indicated were transferred into congenically marked F1 recipients (Ly5.1 x Ly5.2), which were infected with ovalbumin-expressing influenza virus (HKx31-OVA) one day prior to cell transfer. (**a-b)** Flow cytometric analysis of $CD8^+$ T cells in the organs as indicated of influenza infected recipient mice at indicated times after transfer of wildtype and *Irf4*$^{-/-}$ OT-I T cells (left panels), and ratios of donor cells as indicated (right panels). mLN – mediastinal lymph node. (**c)** Cytokine (left) and GzmB (right) expression of donor OT-I T cells of the indicated genotypes as in (b) analysed after restimulation by flow cytometry at indicated time points. (**d)** Expression of CD62L on OT-I T cells of the indicated genotypes at day 5 after infection. **(e)** Ratios (left) and phenotype (right) of OT-I T cells of indicated genotypes. Flow cytometry is representative of 3 independent experiments with 2-3 mice per group. Data points in graphs represent individual mice. Horizontal line shows the mean ±S.E.M.

Figure 4. IRF4 expression and T cell expansion is TCR affinity dependent. (a) Wildtype OT-I T cells were stimulated *in vitro* with different affinity variants of OVA peptide as indicated. IRF4 protein expression was measured by immunoblotting. (**b)** IRF4 expression in donor wildtype OT-I T cells *in vivo* measured by intracellular staining and flow cytometry after infection with HKx31-OVA (N4). (**c)** IRF4

expression in CTV labelled wildtype OT-I T cells 2 or 3 days after transfer in *Listeria*-N4 infected congenically marked recipient mice. (**d)** IRF4 expression in OT-I T cells 5 days after infection with *Listeria* variants as indicated. (**e)** Each $1x10^5$ OT-I T cells of the indicated genotypes were transferred into congenically marked F1 recipients (Ly5.1 x Ly5.2) and subsequently infected with *Listeria*-N4 (Lm-N4) or V4 (Lm-V4). The graph shows proportion of donor T cells in comparison to the endogenous $CD8^+$ T cells in the blood 5 days post infection. (**f-g)** Division profiles as measured by CTV dilution (f) and phenotype (g) of donor OT-I T cells in Lm N4 infected mice at indicated times. (**h)** Expansion of OT-I T cells in response to *Listeria*-N4 (Lm-N4) or V4 (Lm-V4) infection. Data is expressed as a ratio of OT-I T cells present in *Listeria*-N4 (N4) versus V4 infected mice. (**i)** OT-I T cells of the indicated genotypes were stimulated *in vitro* with N4 OVA peptide. Graph shows live cell numbers in culture at indicated times (** $P<0.02$, 2-way ANOVA). Data in (d), (f) and (h) represent cell frequencies in individual mice as indicated from 2-3 individual experiments. Horizontal line shows the mean ±S.E.M. (* $P<0.02$, ** $P<0.002$, *** $P<0.0001$).

Figure 5 IRF4 regulates the affinity-driven transcriptional program in $CD8^+$ T cells. Wildtype (*Irf4*$^{+/+}$) and IRF4-deficient (*Irf4*$^{-/-}$) OT-I $CD8^+$ T cells were activated in the presence of high (N4) or low (V4) affinity peptide for 3 days before being subjected to RNA-sequencing. (**a)** Heatmap of expression levels (normalized log2 fragments per kilobase per million mapped reads) for the top 200 most differentially expressed (DE) genes that are regulated by affinity (*Irf4*$^{+/+}$, V4 versus N4). Full list of genes in Supplementary Table S1. (**b)** Venn-diagram of all DE genes, showing the overlap between TCR affinity-regulated and IRF4-regulated genes. (**c)** Scatterplots of log2-fold changes showing strong correlation between IRF4-dependent changes (x-axis) and affinity-dependent changes (y-axis) when IRF4 is present (left panel, correlation coefficient 0.8) but little correlation when IRF4 is absent (right panel, correlation coefficient 0.16). Plots include all expressed genes. (**d)** Example tracks from RNA sequencing showing affinity and IRF4-dependent repression (*Eomes*) or activation (*S1pr1*), IRF4-independent affinity driven expression (*Ccr2*), and affinity-dependent repressed, IRF4-activated (*Il7r*). (**e-f)** Expression changes between wildtype and *Irf4*-deficient cells stimulated with N4 peptide for selected genes as indicated. Data are the ratio of FPKM values (Log2).

Figure 6 IRF4 binding sites in genes regulating effector and metabolic functions of CD8$^+$ T cells. Wildtype and *Irf4*$^{-/-}$ CD8$^+$ T cells were activated for 3 days *in vitro* in the presence of plate bound anti-CD3, anti-CD28 and IL-2 and subjected to IRF4 ChIP-sequencing (a-d) or metabolic assays (e-i). (**a)** Motif analysis of IRF4 binding sites based on the 1338 most significant peaks ($p<10^{-10}$). The 100 bp sequences centred on the binding summit were used for analysis. (**b)** Motif analysis of IRF4 binding sites based on the 500 most significant peaks. (**c-d)** Examples of ChIP-sequencing tracks showing IRF4 binding in previously known (*Prdm1*, *Il10*), and newly identified target genes. Boxes indicate significant peaks. (**e)** Mitochondrial membrane potential measured by MitoTracker Orange staining of naïve and activated *Irf4*$^{-/-}$ and *Irf4*$^{+/+}$ T cells. (**f-h)** Naïve or for 24 h or 48 h *in vitro* activated CD8$^+$ T cells of the indicated genotypes were subjected to an extracellular flux assay. (**e)** Basal oxygen consumption rate (OCR). (**f)** OCR as a measure of ATP turnover following the addition of 1 μM of oligomycin. (**h)** Basal extracellular acidification rate (ECAR). **i.** Glucose uptake measured by flow cytometry after incubation with the fluorescence labelled glucose analogue 2NB-DG of naive or activated T cells at indicated times. Data in (e) and (i) are representative of two independent experiments. Data in (f-h) are the mean ± S.E.M. from 2-3 biologically independent experiments each performed at least in triplicates (* P<0.003, ** P<0.0001, NS - not significant, N - naive).

Figure 7 IRF4 regulates metabolic function of CD8$^+$ T cells. (**a)** Lactate production of naive or activated T cells at indicated times. **(b)** OCR/ECAR ratio as determined in a mitochondrial stress test of naive or activated CD8$^+$ T cells of the indicated genotypes. (**c)** Change in expression of genes involved in metabolic function in *Irf4*$^{-/-}$ OT-I T cells in comparison to wildtype OT-I T cells after activation with N4 OVA peptide. Data are the ratio of FPKM values (log2) derived by RNA-sequencing; * indicates genes bound directly by IRF4. (**d)** Examples of ChIP-sequencing tracks showing IRF4 binding at the indicated loci. Boxes indicate significant peaks. (**e)** Transcript levels of genes involved in OXPHOS (upper panel) and glycolysis (lower panel) in OT-I T cells of the indicated genotypes activated with N4 peptide, determined by quantitative RT-PCR. The graphs show expression relative to naïve

cells and are representative of two biologically independent experiments performed in triplicates. Data are mean ± S.D. (**f)** Immunoblot analysis of naive or activated $CD8^+$ T cells as indicated, representative of two independent experiments. Data in (a) and (b) are the mean ± S.E.M. of 2 biologically independent experiments each performed in triplicates (* P<0.04, ** P<0.007, *** P<0.0001, NS - not significant, N - naive).

Figure 8 IRF4 regulates metabolic function of $CD8^+$ T cells *in vivo* and can rescue low affinity T cell responses. (**a)** Extracellular flux analysis of donor OT-I T cells of the indicated genotypes at day 4 post *Listeria*-N4 infection. (**b)** ECAR measured in a glycolytic stress. (**c)** OCR/ECAR ratio as in (a). (**d)** Glucose uptake of OT-I T cells of the indicated genotypes isolated from mice infected with *Listeria* strains as indicated, measured by flow cytometry after incubation with the fluorescently labelled glucose analogue 2NB-DG (day 3). (**e)** Lactate production of naive T cells or OT-I T cells of the indicated genotypes sorted from mice infected with recombinant *Listeria* expressing high (Lm-N4) or low-affinity OVA peptide (Lm-V4) three days previously. (**f-g)** Forward scatter as a measure of size of OT-I T cells of the indicated genotypes (f), and expression of CD71 in response to infection with *Listeria* strains as indicated (g) at day 3 after infection. (**h)** Rescue of T cells responding to a low-affinity antigen by over expression of IRF4. $2x10^4$ wildtype OT-I T cells (Ly5.2) transduced with an IRF4 overexpressing (IRF4-GFP) or control (GFP) retrovirus as indicated were adoptively transferred into congenically marked recipient mice, which were infected with *Listeria* V4. Flow cytometry of $CD8^+$ T cells in the blood 6 days post infection (left), quantitation (right). Flow plots in (d), (g), (h) are representative for at least 2 biologically independent experiments containing each 3-4 mice. Graphs in (a), (c) and d-h are the mean ±S.E.M. from 2-3 biologically independent experiments each performed at least in triplicates (* P<0.02, ** P<0.002, *** P<0.0002, NS - not significant).

Experimental Procedures

Mouse models. *Irf4*$^{-/-}$ mice were described previously[23] and maintained on a C57BL/6 (Ly5.2) background. For some of the experiments they were crossed to OT-I TCR transgenic[34], *Bim*$^{-/-}$[33], *Vav-Bcl2*tg[32], GzmBCre[31] or *Prdm1*^{GFP}[51] mice. Mixed bone marrow chimeras were generated from lethally irradiated (2 x 550R) wildtype Ly5.1 mice reconstituted with a mixture of mutant or control bone marrow (Ly5.2) and Ly5.1 bone marrow as indicated and mice were allowed 6-8 weeks to reconstitute. Mice were maintained and used in accordance with the guidelines of the Walter and Eliza Hall Institute Animal Ethics Committee.

Infections. Mice were anaesthetized with methoxyfluorane and then inoculated with 10^4 plaque forming units (p.f.u.) of the HKx31 (H3N2) influenza virus[52,53]. In some experiments mice were first inoculated i.p. with 10^7 p.f.u. of the heterologous influenza virus A/PR/8/34 (H1N1, PR8, Mt Sinai strain) 4-6 weeks prior to the infection with HKx31. Lymphocytic choriomeningitis virus (LCMV) infections were done by intravenous injection of $3x10^3$ p.f.u (WE strain).

To measure responses of OT-I TCR transgenic $CD8^+$ T cells mice were infected with either recombinant HKx31 (H3N2) virus expressing an OVA peptide (1.5×10^4 p.f.u.)[35], or with *Listeria monocytogenes* expressing altered affinity OVA peptide variants ($2.5x10^3$ p.f.u.) as previously described[17]. 24 hours later $5x10^5$ OT-I-TCR transgenic $CD8^+$ T cells were transferred into infected animals by intravenous injection.

Retroviral overexpression of IRF4. Retroviral supernatant was produced from HEK293 T cells transfected with retroviral expression plasmids (pMSCV) containing either a GFP or IRF4-IRES-GFP expression cassette. For retroviral transduction naïve $CD8^+$ T cells were isolated from spleens and lymph nodes of OTI transgenic mice and activated *in vitro* with OVA peptides N4 (SIINFEKL) or V4 (SIIVFEKL) (1 μg/ml) in the presence of recombinant human IL-2 (100 u/ml, R&D systems) for 48 hours before spin infection. After 24 hours, GFP^+ cells were sorted (BD Aria W) and re-cultured in recombinant human IL-15 (50 μg/ml) (R&D Systems) for 4 days. $2x10^4$

cells were then adoptively transferred into naïve Ly5.1 recipients, which were infected with *Listeria* OVA on the same day.

Tetramers and intracellular cytokine staining. LCMV specific $CD8^+$ T cell responses were enumerated with MHC class I (H-$2D^b$) tetramers complexed with either LCMV–$GP_{33–41}$ (GP_{33}) or LCMV–$NP_{396–404}$ (NP_{396}) peptides were from Baylor College of Medicine, Houston, Texas. Influenza (HKx31) specific responses were enumerated by staining with phycoerythrin (PE)-labeled MHC class I tetrameric complexes specific for the two H-2^b-restricted immunodominant epitopes of influenza virus, namely the nucleoprotein (NP_{366}; $D^bNP_{366-374}$) and acid polymerase (PA_{224}; $D^bPA_{224-233}$)[53].

Restimulations were performed using either phorbol 12-myristate 13-acetate (PMA, 50 □g/ml) and ionomycin (0.5 □g/ml), or antigen-specific peptides (LCMV, GP_{33} and NP_{396}; HKx31, NP_{366} and PA_{224}) or N4 OVA peptide (1 μg/ml) in the presence of GolgiPlug (BD Bioscience) for 5 hours. Intracellular staining of cytokines and granzyme B was performed using the BD kit, staining of transcription factor was performed using the FoxP3 staining kit (eBioscience) according to manufacturers protocols.

Antibodies and flow cytometry. Fluorochrome-conjugated antibodies directed against the following antigens were used for analysis by flow cytometry: CD8α (53-6.7), CD62L (MEL-14), KLRG1 (2F1), IL-7R (A7R34), CD25 (PC61.5), Eomes (Dan11mag), CD71 (R17217) (from eBiosicence), Ly5.1 (A20), Ly 5.2 (104), CD44 (IM7), IFNγ (XMG1.2), TNFα (MP5-XT22), IL-2 (JES6-5H4), CD138 (281-2), CD69 (H1.2F3) (from BD Pharmingen), GzmB (GB12, Invitrogen), and IRF4 (M17) and normal goat IgG (from Santa Cruz Biotech). Propidium iodide or SytoxBlue (Invitrogen) was used to exclude dead cells. In some experiments $CD8^+$ T cells were enriched prior to analysis by depletion using antibodies against CD11b (M1/70), F4/80 (F4/80), Ter-119, Gr-1 (RB6-8C5), MHCII (M5/114), and CD4 (GK1.5). Intracellular staining for IRF4 used a donkey anti-goat IgG FITC from Jackson ImmunoResearch Laboratories. Active Caspase 3 (BD Pharmingen) intracellular staining was performed using the FoxP3 staining kit (eBioscience) according to the manufacturers protocols. Annexin V staining (BD Pharmingen) was performed in

buffered solution containing 25 mM calcium chloride at room temperature for 20 min prior to analysis by flow cytometry.

Cell Culture and Metabolic Assays. OT-I TCR transgenic cells were stimulated with OVA peptides (1 □g/ml) in the presence of IL-2 (100 U/ml). $CD8^+$ T cells were cultured using plate bound anti-CD3, soluble anti-CD28 antibodies and recombinant human IL-2 (rhIL-2) as previously described.

For extracellular flux assays, activated cells were harvested at indicated times after the start of the culture and rested in IL-2 (100 U/ml) overnight. Subsequently dead cells were removed by Ficoll gradient centrifugation. Naïve T cells were cultured in IL-7 for 24 h prior to metabolic assays. Immediately prior to the assay, 750,000 cells were seeded per well and the plate centrifuged at 2000 rpm for 20 mins so that the cells would adhere to the bottom of the plate. Oxygen consumption rates (OCR) and extracellular acidification rates (ECAR) were measured in DMEM containing 1 mM L-Ala-Gln (glutamax), 1 mM sodium pyruvate and 25 mM glucose, under basal conditions and in response to 1 μM oligomycin, 1 μM fluorocarbonyl cyanide phenylhydrazone (FCCP), 1 μM rotenone and 1 μM antimycin A with the XF-24 Extracellular Flux Analyzer (Searhorse Bioscience). OCR and ECAR values from the extracellular flux assays stress test were calculated as described[54,55]. Glycolytic Stress Tests were carried out as described above, except that cells were resuspended in glucose and pyruvate-free DMEM before the addition of 10 mM glucose, 1 μM oligomycin and 50 mM 2-DG during the assay.

To determined glucose uptake *ex vivo* splenocytes from *Listeria*-OVA infected mice day 3 post infection were incubated with 30 μM of a fluorescence labelled glucose analogue (2-NBDG, Invitrogen) for 2 h in glucose-free RPMI and washed twice with PBS before staining with labelled antibodies against cell surface proteins. Fluorescence was determined by flow cytometry. To determine glucose uptake *in vitro*, naïve CD8+ T cells were activated with anti-CD3 and recombinant IL-2 or cultured with IL-7 before incubation with 2NB-DG for 1 h and subsequent analysis by flow cytometry.

Extracellular L-lactate concentration were determined as follows: OT-I T cells were flow sorted from Listeria-OVA infected mice three days post infection and were recultured overnight at a density of $5x10^5$ cells/ml in complete RPMI before

extracellular L-lactate concentrations were determined using the Glycolysis Cell-Based Assay Kit (Cayman Chemical) according to manufacturers protocols.

Chromatin Immunoprecipitation (ChIP)-Seq and bioinformatic analysis. ChIP was performed following an adapted protocol by Upstate/Milipore (Massachusetts, USA). In brief, naïve $CD8^+$ T cells isolated from spleens and lymph nodes were stimulated *in vitro* with anti-CD3 (5 μg/ml), anti-CD28 (1.8 μg/ml) and rhIL-2 (100 U/ml) for 72 h. Live cells were isolated by Histopaque gradient centrifugation. Cross-linking was done by addition of 1% paraformaldehyde at room temperature for 10 min, followed by sonication and immunoprecipitation with 10 μg of anti-IRF4 (clone sc-6059) and a corresponding goat polyclonal-IgG control (clone sc-2028) (Santa Cruz Technologies). The DNA fragments were blunt-end ligated to the Illumina adaptors, amplified, and sequenced with the HiSeq Genome Analyzer (Illumina). Single-end sequenced reads of 49 bp were obtained with the Illumina Analysis Pipeline and mapped to the mouse genome (mm9) using the Subread aligner[56]. Ten subreads were extracted from each read and at least three consensus subreads were required to report a hit. Mapping quality scores were used to break the tie when more than one best locations were found for a read. Only uniquely mapped reads were retained. Supplementary Table S2 gives the total number of reads and percentage of reads for the ChIP and input control libraries. IRF4 binding peaks were identified using MACS v1.4.1 program[57] with a p-value cutoff of 10^{-5}, with total sonicated chromatin (input) used as a control. Genes with binding peaks falling within between 20 kilobases upstream and 5 kilobases downstream of the gene body were considered to be IRF4 binding targets. NCBI RefSeq mouse annotation build 37.2 was used to obtain chromosomal coordinates of genes. Entrez gene identifiers were used to match genes in ChIP-seq data with those in RNA-seq data. MEME v4.8.1 program was used to carry out a *de novo* motif discovery to find the binding co-factors of IRF4. 100 bp genomic sequences centered on IRF4 binding summit positions were used for motif search.

RNA-sequencing and bioinformatic analysis. Naïve $CD8^+$ T cells were isolated from spleens and lymph nodes of OT-I transgenic mice and activated in vitro with OVA peptides N4 and V4 (1 μg/ml), respectively, and rhIL-2 (100 U/ml) for 72 h.

RNA purification was performed following the manufacturer's protocol using the RNAeasy Plus Mini Kit (Qiagen). Reads were mapped as for ChIP-seq except for that paired-end information was used. The distance between paired reads was constrained to be 50−600 bp. Subsequent analysis used Bioconductor software[58]. The featureCounts function of the Rsubread package was used to count the number of fragments mapped to the exome of each gene. Fragments overlapping exons in the NCBI RefSeq mouse annotation build 37.2 were included. Supplementary Table S2 gives the total number of reads, percentage of reads mapped to mouse and percentage of reads assigned to genes for each RNA sample. Genes were filtered from downstream analysis if they failed to achieve at least 8 FPKM (Fragments Per Kilobases per Million mapped reads) in at least one library. Counts were converted to log2 counts per million, quantile normalized and precision weighted using the voom function of the limma package[59]. A linear model was fitted to each gene and empirical Bayes moderated *t*-statistics were used to assess differential expression[60]. P-values were adjusted to control the global false discovery rate (FDR) across all comparisons using the global option of the limma package. Heatmaps were generated using the gplots package, with negative log2 FPKM values reset to zero.

Immunoblotting. Whole cell extracts were produced by cell lysis in RIPA buffer containing standard protease inhibitors. Proteins were resolved by denaturing SDS-PAGE and transferred onto nitrocellulose membrane. The following primary antibodies were used, anti-IRF4[26], anti-Myc (Cell Signalling) and anti-β-actin (I-19, Santa Cruz).

Statistics. If not stated otherwise a paired or unpaired student t test as appropriate was performed to test for statistical significance.

Ingenuity Pathway Analysis (IPA). The differentially expressed genes for *Irf4*$^{-/-}$ vs *Irf4*$^{+/+}$ from the N4 RNA-seq data were functionally analyzed using the knowledge database IPA (Ingenuity Systems, version 11631407, date of analysis 1 April 2013, www.ingenuity.com). IPA can design molecular networks of inter-related genes based on previously published data and can assign the most important functionalities to

these networks. We set IPA to build networks based on both direct and indirect relationships with our differentially expressed genes.

References

1 Belz, G. T. & Kallies, A. Effector and memory CD8+ T cell differentiation: toward a molecular understanding of fate determination. *Curr Opin Immunol* **22**, 279-285 (2010).

2 Kaech, S. M. & Cui, W. Transcriptional control of effector and memory CD8(+) T cell differentiation. *Nature reviews. Immunology* **12**, 749-761 (2012).

3 Intlekofer, A. M. *et al.* Effector and memory CD8+ T cell fate coupled by T-bet and eomesodermin. *Nature immunology* **6**, 1236-1244 (2005).

4 Kallies, A., Xin, A., Belz, G. T. & Nutt, S. L. Blimp-1 transcription factor is required for the differentiation of effector CD8(+) T cells and memory responses. *Immunity* **31**, 283-295 (2009).

5 Rutishauser, R. L. *et al.* Transcriptional repressor Blimp-1 promotes CD8(+) T cell terminal differentiation and represses the acquisition of central memory T cell properties. *Immunity* **31**, 296-308 (2009).

6 Yang, C. Y. *et al.* The transcriptional regulators Id2 and Id3 control the formation of distinct memory CD8+ T cell subsets. *Nature immunology* **12**, 1221-1229 (2011).

7 Cannarile, M. A. *et al.* Transcriptional regulator Id2 mediates CD8+ T cell immunity. *Nature immunology* **7**, 1317-1325 (2006).

8 Gett, A. V., Sallusto, F., Lanzavecchia, A. & Geginat, J. T cell fitness determined by signal strength. *Nature immunology* **4**, 355-360 (2003).

9 Day, E. K. *et al.* Rapid CD8+ T cell repertoire focusing and selection of high-affinity clones into memory following primary infection with a persistent human virus: human cytomegalovirus. *Journal of immunology* **179**, 3203-3213 (2007).

10 Price, D. A. *et al.* Avidity for antigen shapes clonal dominance in CD8+ T cell populations specific for persistent DNA viruses. *The Journal of experimental medicine* **202**, 1349-1361 (2005).

11 Malherbe, L., Hausl, C., Teyton, L. & McHeyzer-Williams, M. G. Clonal selection of helper T cells is determined by an affinity threshold with no further skewing of TCR binding properties. *Immunity* **21**, 669-679 (2004).

12 Busch, D. H. & Pamer, E. G. T cell affinity maturation by selective expansion during infection. *The Journal of experimental medicine* **189**, 701-710 (1999).

13 Savage, P. A., Boniface, J. J. & Davis, M. M. A kinetic basis for T cell receptor repertoire selection during an immune response. *Immunity* **10**, 485-492 (1999).

14 Alexander-Miller, M. A., Leggatt, G. R. & Berzofsky, J. A. Selective expansion of high- or low-avidity cytotoxic T lymphocytes and efficacy for

adoptive immunotherapy. *Proceedings of the National Academy of Sciences of the United States of America* **93**, 4102-4107 (1996).
15 Schmitz, J. E. *et al.* Control of viremia in simian immunodeficiency virus infection by CD8+ lymphocytes. *Science* **283**, 857-860 (1999).
16 Shoukry, N. H. *et al.* Memory CD8+ T cells are required for protection from persistent hepatitis C virus infection. *The Journal of experimental medicine* **197**, 1645-1655 (2003).
17 Zehn, D., Lee, S. Y. & Bevan, M. J. Complete but curtailed T-cell response to very low-affinity antigen. *Nature* **458**, 211-214 (2009).
18 King, C. G. *et al.* T cell affinity regulates asymmetric division, effector cell differentiation, and tissue pathology. *Immunity* **37**, 709-720 (2012).
19 Wensveen, F. M. *et al.* Apoptosis threshold set by Noxa and Mcl-1 after T cell activation regulates competitive selection of high-affinity clones. *Immunity* **32**, 754-765 (2010).
20 Teixeiro, E. *et al.* Different T cell receptor signals determine CD8+ memory versus effector development. *Science* **323**, 502-505 (2009).
21 Smith-Garvin, J. E. *et al.* T-cell receptor signals direct the composition and function of the memory CD8+ T-cell pool. *Blood* **116**, 5548-5559 (2010).
22 Sarkar, S. *et al.* Strength of stimulus and clonal competition impact the rate of memory CD8 T cell differentiation. *Journal of immunology* **179**, 6704-6714 (2007).
23 Mittrucker, H. W. *et al.* Requirement for the transcription factor LSIRF/IRF4 for mature B and T lymphocyte function. *Science* **275**, 540-543 (1997).
24 Klein, U. *et al.* Transcription factor IRF4 controls plasma cell differentiation and class-switch recombination. *Nat. Immunol* **7**, 773-782 (2006).
25 Sciammas, R. *et al.* Graded expression of interferon regulatory factor-4 coordinates isotype switching with plasma cell differentiation. *Immunity* **25**, 225-236 (2006).
26 Zheng, Y. *et al.* Regulatory T-cell suppressor program co-opts transcription factor IRF4 to control T(H)2 responses. *Nature* **458**, 351-356 (2009).
27 Cretney, E. *et al.* The transcription factors Blimp-1 and IRF4 jointly control the differentiation and function of effector regulatory T cells. *Nature immunology* **12**, 304-311 (2011).
28 Brustle, A. *et al.* The development of inflammatory T(H)-17 cells requires interferon-regulatory factor 4. *Nature immunology* (2007).
29 Staudt, V. *et al.* Interferon-regulatory factor 4 is essential for the developmental program of T helper 9 cells. *Immunity* **33**, 192-202 (2010).
30 Kwon, H. *et al.* Analysis of interleukin-21-induced Prdm1 gene regulation reveals functional cooperation of STAT3 and IRF4 transcription factors. *Immunity* **31**, 941-952 (2009).
31 Jacob, J. & Baltimore, D. Modelling T-cell memory by genetic marking of memory T cells in vivo. *Nature* **399**, 593-597 (1999).
32 Ogilvy, S. *et al.* Constitutive Bcl-2 expression throughout the hematopoietic compartment affects multiple lineages and enhances progenitor cell survival. *Proceedings of the National Academy of Sciences of the United States of America* **96**, 14943-14948 (1999).

33 Bouillet, P. *et al.* Proapoptotic Bcl-2 relative Bim required for certain apoptotic responses, leukocyte homeostasis, and to preclude autoimmunity. *Science* **286**, 1735-1738 (1999).
34 Hogquist, K. A. *et al.* T cell receptor antagonist peptides induce positive selection. *Cell* **76**, 17-27 (1994).
35 Seah, S. G. *et al.* Unlike CD4+ T-cell help, CD28 costimulation is necessary for effective primary CD8+ T-cell influenza-specific immunity. *European journal of immunology* **42**, 1744-1754 (2012).
36 Gronski, M. A. *et al.* TCR affinity and negative regulation limit autoimmunity. *Nat Med* **10**, 1234-1239 (2004).
37 Cruz-Guilloty, F. *et al.* Runx3 and T-box proteins cooperate to establish the transcriptional program of effector CTLs. *The Journal of experimental medicine* **206**, 51-59 (2009).
38 Kerdiles, Y. M. *et al.* Foxo1 links homing and survival of naive T cells by regulating L-selectin, CCR7 and interleukin 7 receptor. *Nature immunology* **10**, 176-184 (2009).
39 Rao, R. R., Li, Q., Gubbels Bupp, M. R. & Shrikant, P. A. Transcription factor Foxo1 represses T-bet-mediated effector functions and promotes memory CD8(+) T cell differentiation. *Immunity* **36**, 374-387 (2012).
40 Finlay, D. K. *et al.* PDK1 regulation of mTOR and hypoxia-inducible factor 1 integrate metabolism and migration of CD8+ T cells. *The Journal of experimental medicine* **209**, 2441-2453 (2012).
41 Li, P. *et al.* BATF-JUN is critical for IRF4-mediated transcription in T cells. *Nature* **490**, 543-546 (2012).
42 Ciofani, M. *et al.* A validated regulatory network for Th17 cell specification. *Cell* **151**, 289-303 (2012).
43 Glasmacher, E. *et al.* A Genomic Regulatory Element That Directs Assembly and Function of Immune-Specific AP-1-IRF Complexes. *Science* **338**, 975-980 (2012).
44 MacIver, N. J., Michalek, R. D. & Rathmell, J. C. Metabolic regulation of T lymphocytes. *Annual review of immunology* **31**, 259-283 (2013).
45 Finlay, D. & Cantrell, D. A. Metabolism, migration and memory in cytotoxic T cells. *Nature reviews. Immunology* **11**, 109-117 (2011).
46 van der Windt, G. J. & Pearce, E. L. Metabolic switching and fuel choice during T-cell differentiation and memory development. *Immunological reviews* **249**, 27-42 (2012).
47 Wang, R. & Green, D. R. Metabolic checkpoints in activated T cells. *Nature immunology* **13**, 907-915 (2012).
48 Wang, R. *et al.* The transcription factor Myc controls metabolic reprogramming upon T lymphocyte activation. *Immunity* **35**, 871-882 (2011).
49 Chang, C. H. *et al.* Posttranscriptional control of T cell effector function by aerobic glycolysis. *Cell* **153**, 1239-1251 (2013).
50 Tothova, Z. *et al.* FoxOs are critical mediators of hematopoietic stem cell resistance to physiologic oxidative stress. *Cell* **128**, 325-339 (2007).
51 Kallies, A. *et al.* Plasma cell ontogeny defined by quantitative changes in blimp-1 expression. *The Journal of experimental medicine* **200**, 967-977 (2004).

52 Flynn, K. J. *et al.* Virus-specific CD8+ T cells in primary and secondary influenza pneumonia. *Immunity* **8**, 683-691 (1998).

53 Belz, G. T., Xie, W., Altman, J. D. & Doherty, P. C. A previously unrecognized H-2D(b)-restricted peptide prominent in the primary influenza A virus-specific CD8(+) T-cell response is much less apparent following secondary challenge. *J Virol* **74**, 3486-3493 (2000).

54 Ritchie, R. H. *et al.* Enhanced phosphoinositide 3-kinase(p110alpha) activity prevents diabetes-induced cardiomyopathy and superoxide generation in a mouse model of diabetes. *Diabetologia* **55**, 3369-3381 (2012).

55 Wu, M. *et al.* Multiparameter metabolic analysis reveals a close link between attenuated mitochondrial bioenergetic function and enhanced glycolysis dependency in human tumor cells. *American journal of physiology. Cell physiology* **292**, C125-136 (2007).

56 Liao, Y., Smyth, G. K. & Shi, W. The Subread aligner: fast, accurate and scalable read mapping by seed-and-vote. *Nucleic acids research* **41**, e108, (2013).

57 Zhang, Y., Liu, T., Meyer, C.A., Eeckhoute, J., Johnson, D.S., Bernstein, B.E., Nusbaum, C., Myers, R.M., Brown, M., Li, W., and Liu, X.S. Model-based analysis of ChIP-Seq (MACS). *Genome Biol.* **9**, R137 (2008).

58 Gentleman, R. C., Carey, V.J., Bates, D.M., Bolstad, B., Dettling, M., Dudoit, S., Ellis, B., Gautier, L., Ge, Y., Gentry, J., et al. Bioconductor: open software development for computational biology and bioinformatics. *Genome Biol.* **5** (2004).

59 Smyth, G. K. Limma: linear models for microarray data. In: 'Bioinformatics and Computational Biology Solutions using R and Bioconductor. *R. Gentleman, V. Carey, S. Dudoit, R. Irizarry, W. Huber (eds), Springer, New York, pp 397-420*. (2005).

60 Smyth, G. K. Linear models and empirical Bayes methods for assessing differential expression in microarray experiments. *Statistical Applications in Genetics and Molecular Biology* **3** (2004).

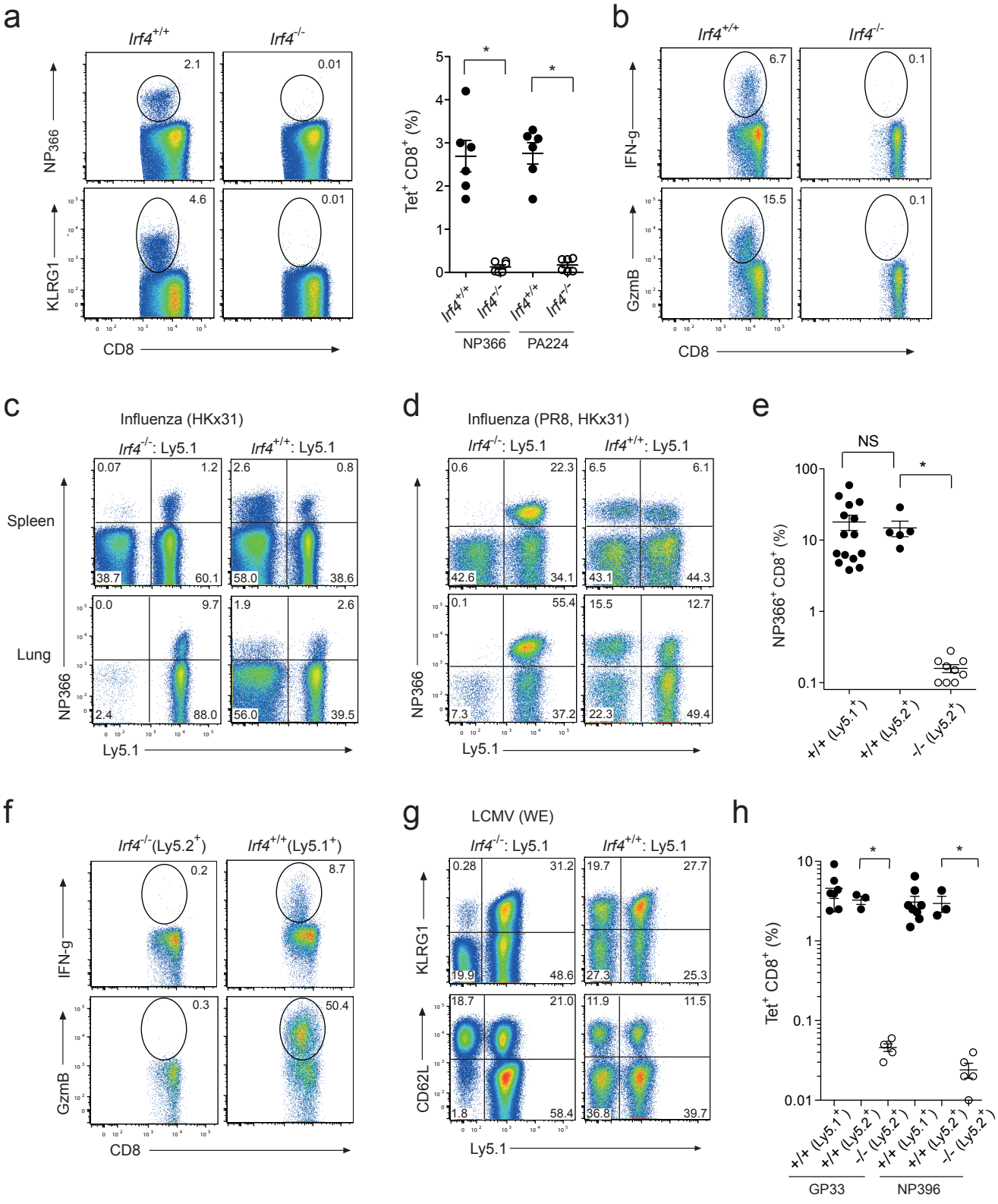

Man et al. Fig. 1

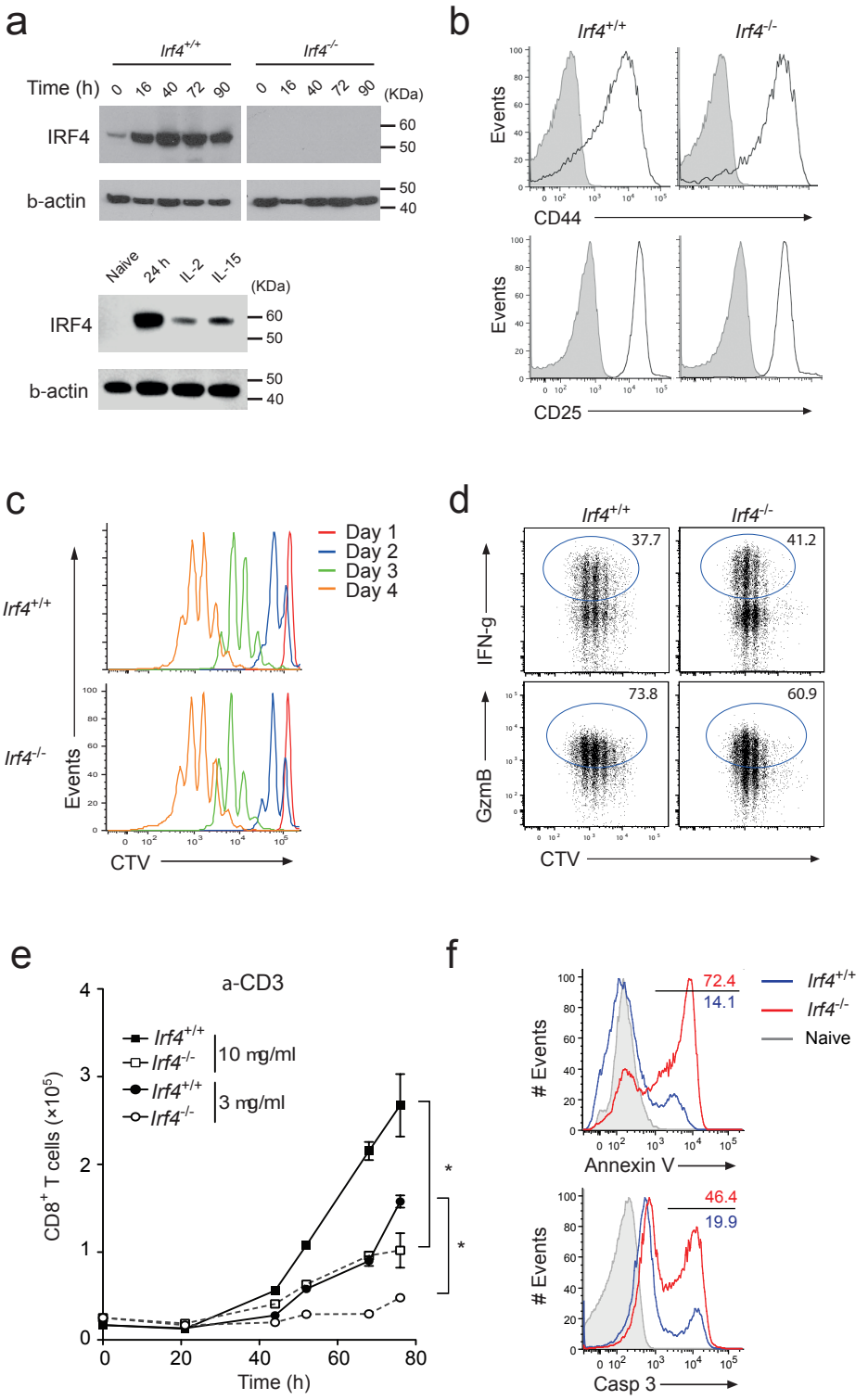

Man et al. Fig. 2

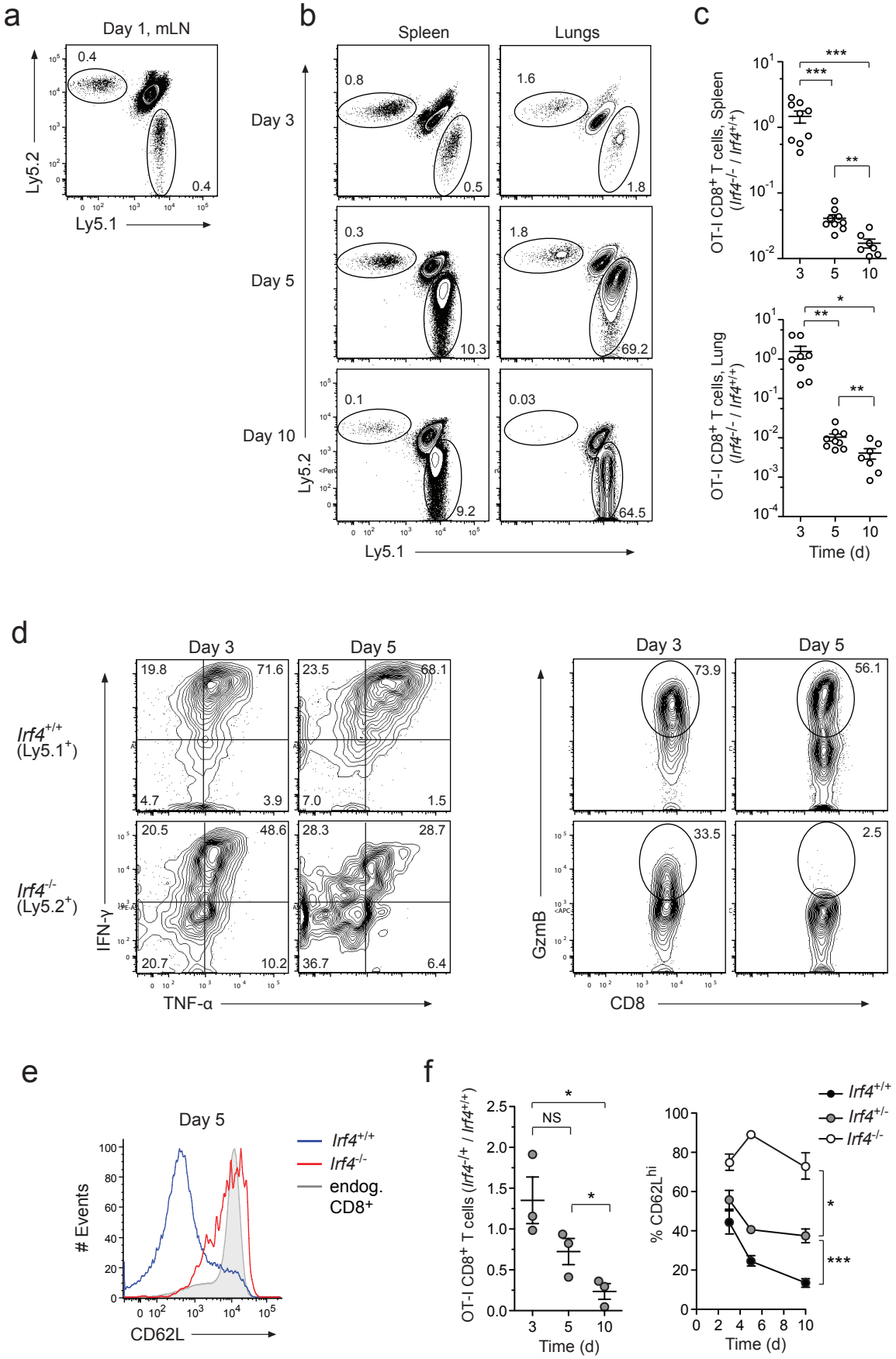

Man et al. Fig. 3

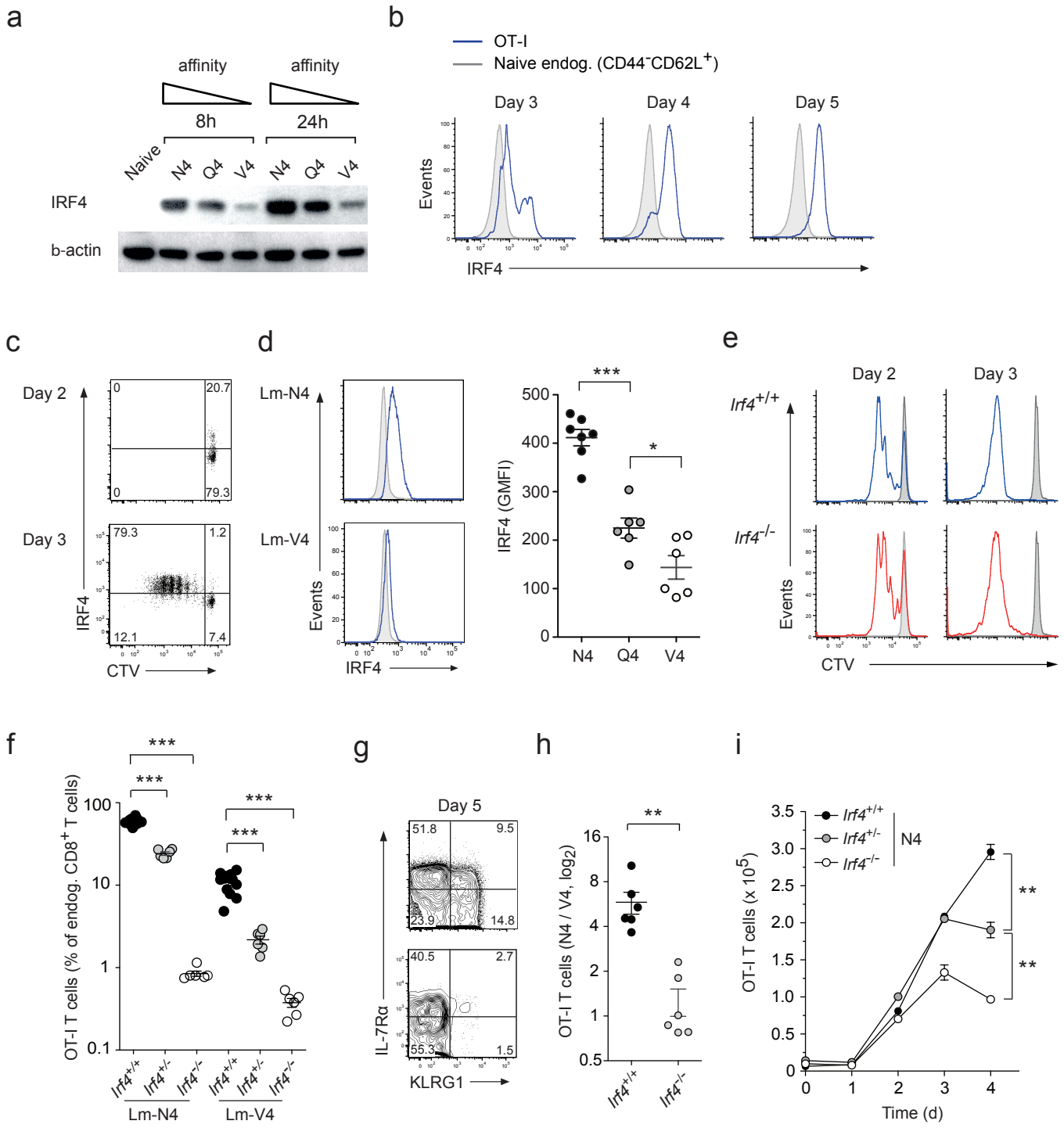

Man et al. Fig. 4

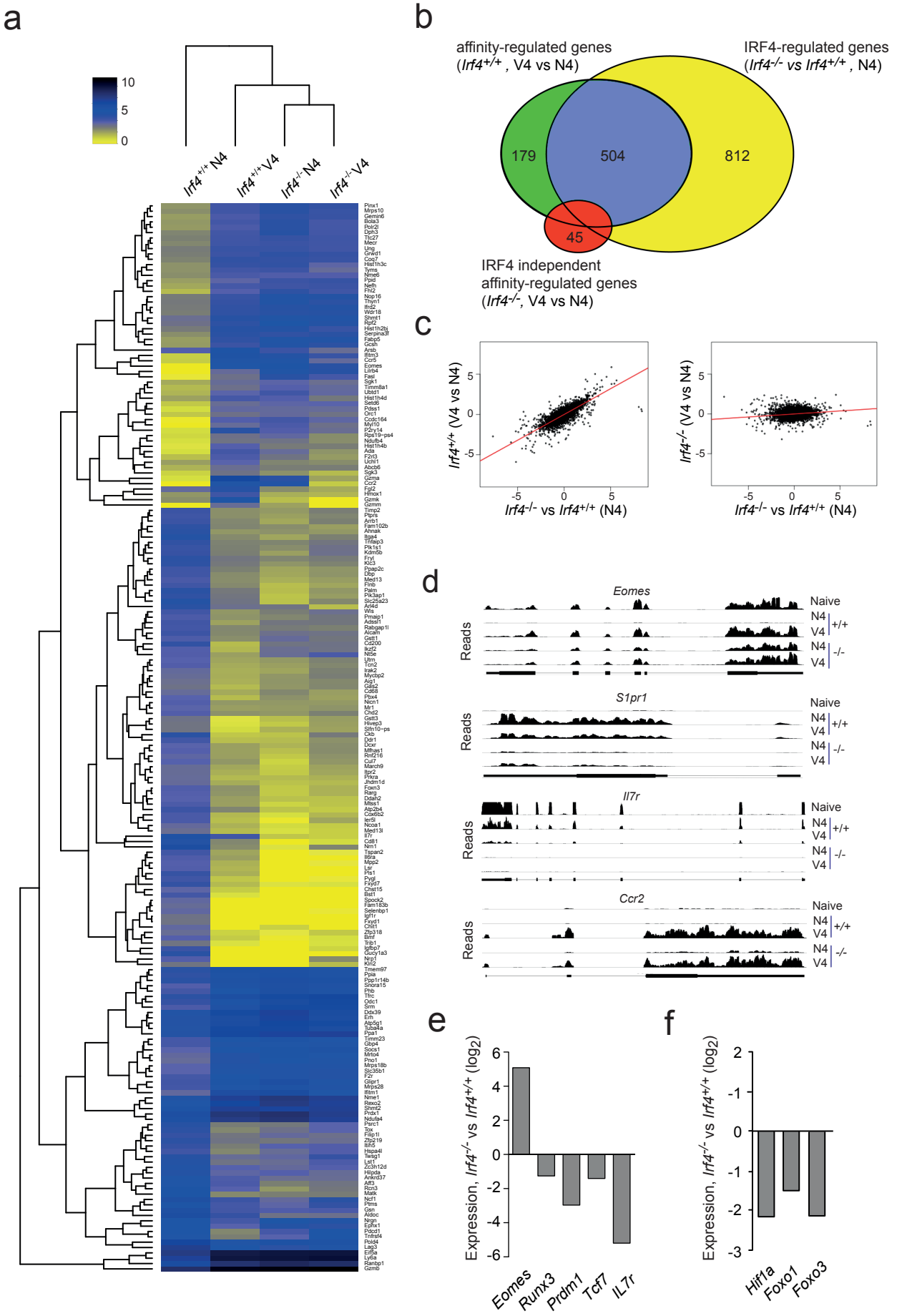

Man et al. Fig. 5

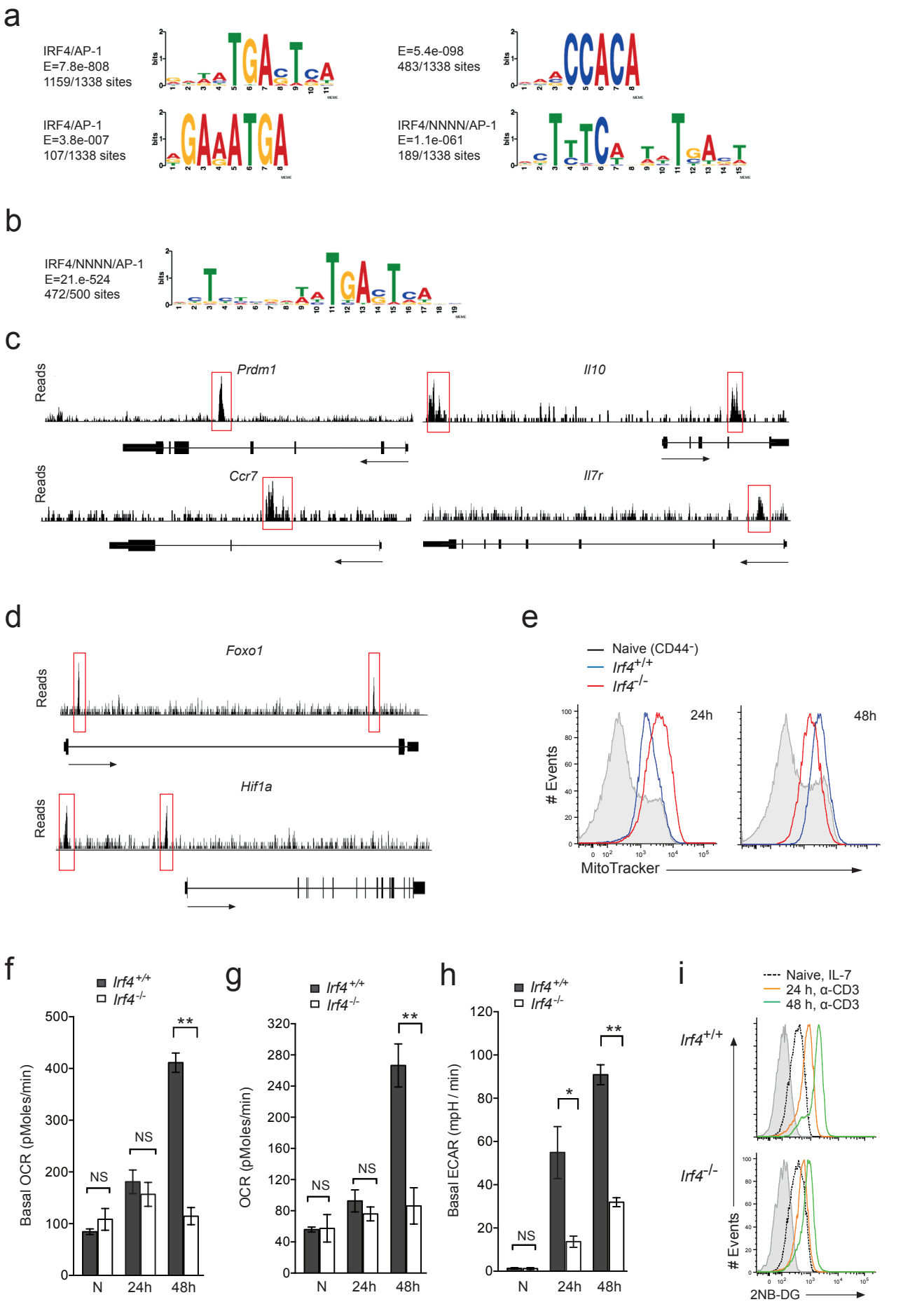

Man et al. Fig. 6

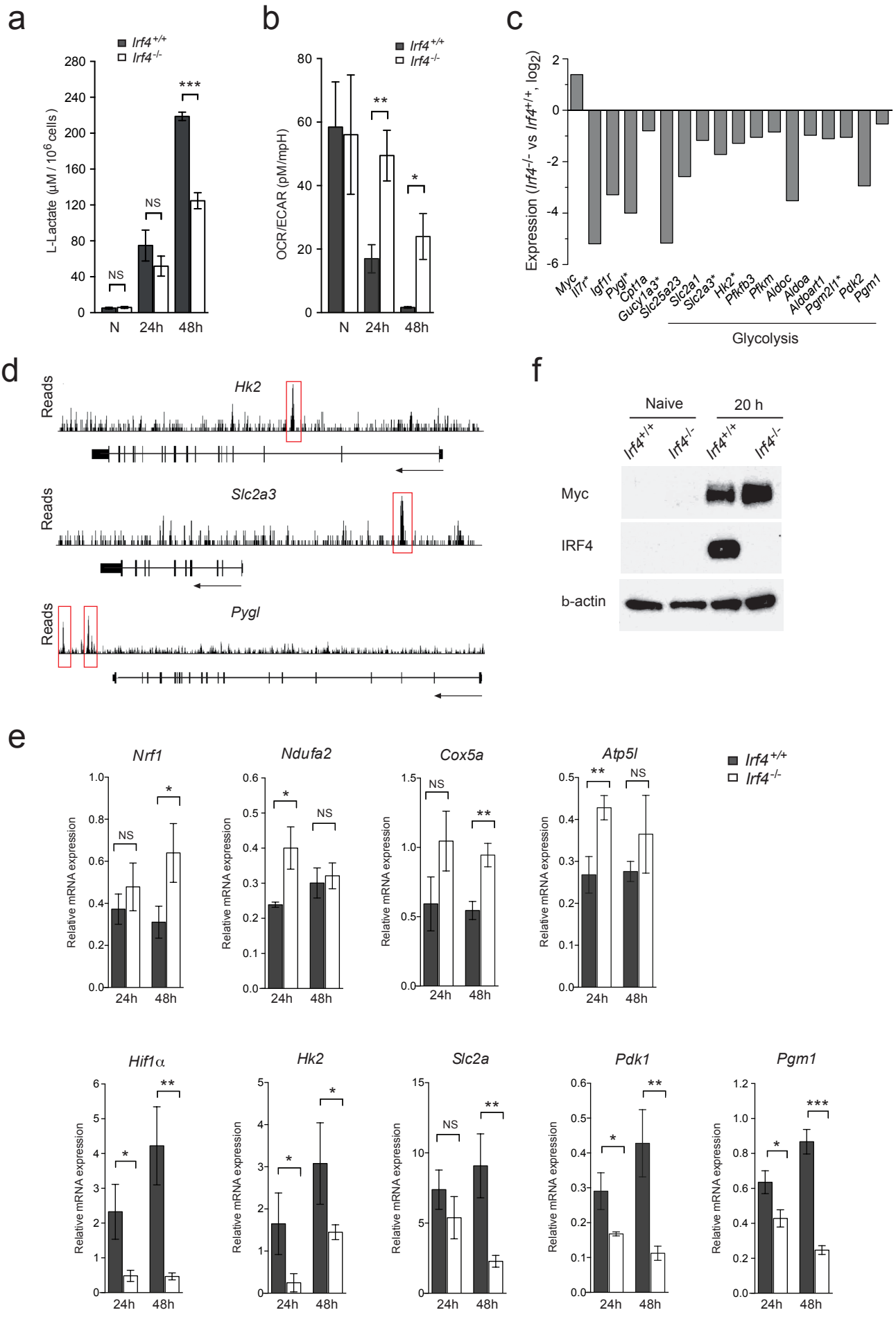

Man et al. Fig. 7

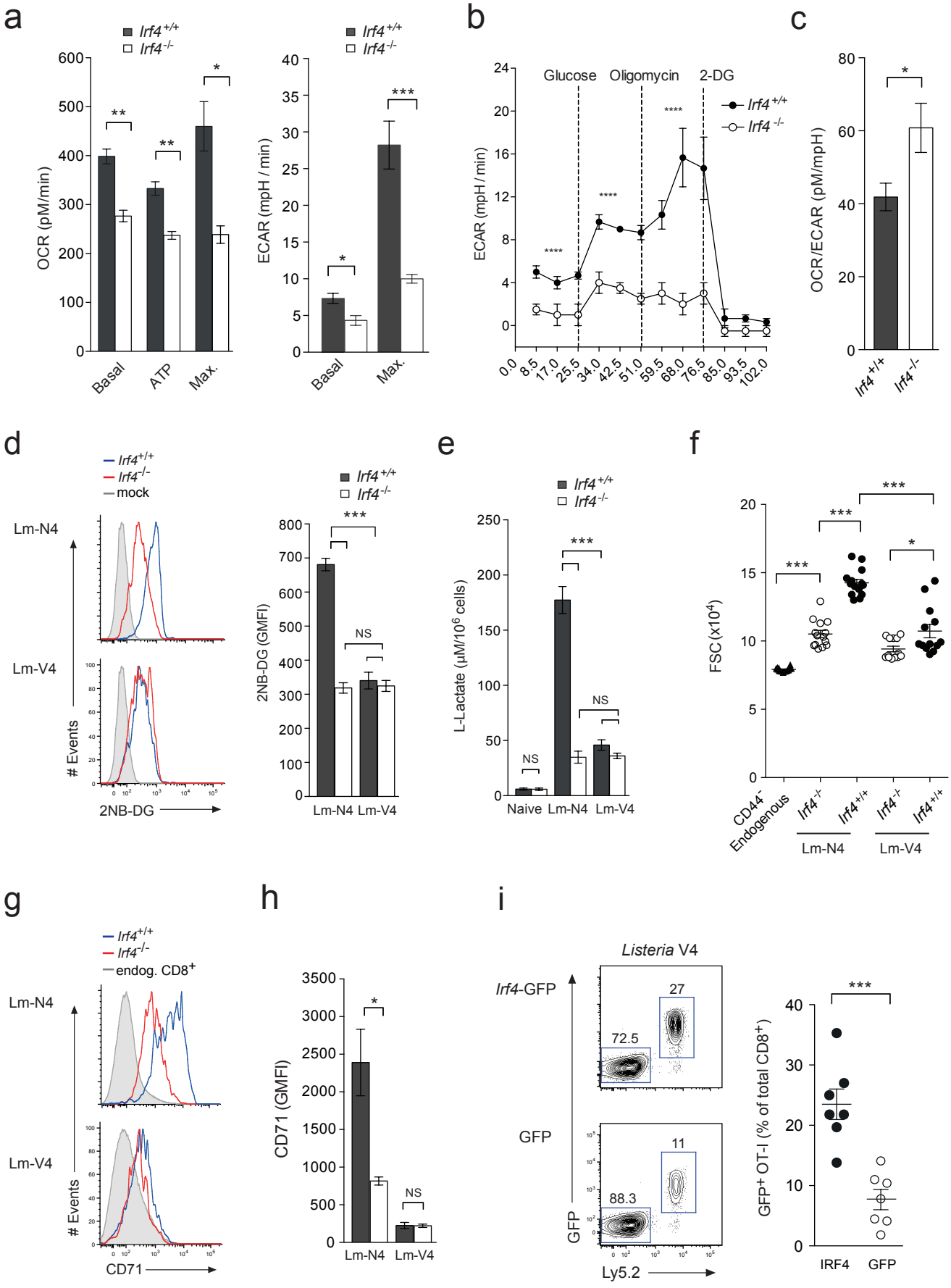

Man et al. Fig. 8

Supplementary Information

The transcription factor IRF4 is essential for T cell receptor affinity mediated metabolic programming and clonal expansion of T cells

Kevin Man[1,2], Maria Miasari[1,2], Wei Shi[1,3], Annie Xin[1,2], Darren C. Henstridge[5], Simon Preston[1,2], Marc Pellegrini[1,2], Gabrielle T. Belz[1,2], Gordon K. Smyth[1,4], Mark A. Febbraio[5], Stephen L. Nutt[1,2], Axel Kallies[1,2]

[1] The Walter and Eliza Hall Institute of Medical Research, 1G Royal Parade, Parkville, Victoria, 3050, Australia.

[2] The Department of Medical Biology, University of Melbourne, Parkville, Victoria, 3010, Australia.

[3] The Department of Computing and Information Systems, University of Melbourne, Parkville, Victoria, 3010, Australia.

[4] The Department of Mathematics and Statistics, University of Melbourne, Parkville, Victoria, 3010, Australia.

[5] Cellular and Molecular Metabolism Laboratory, Baker IDI Heart and Diabetes Institute, Melbourne, Victoria, 3004, Australia.

Correspondence should be addressed to A.K. (kallies@wehi.edu.au).

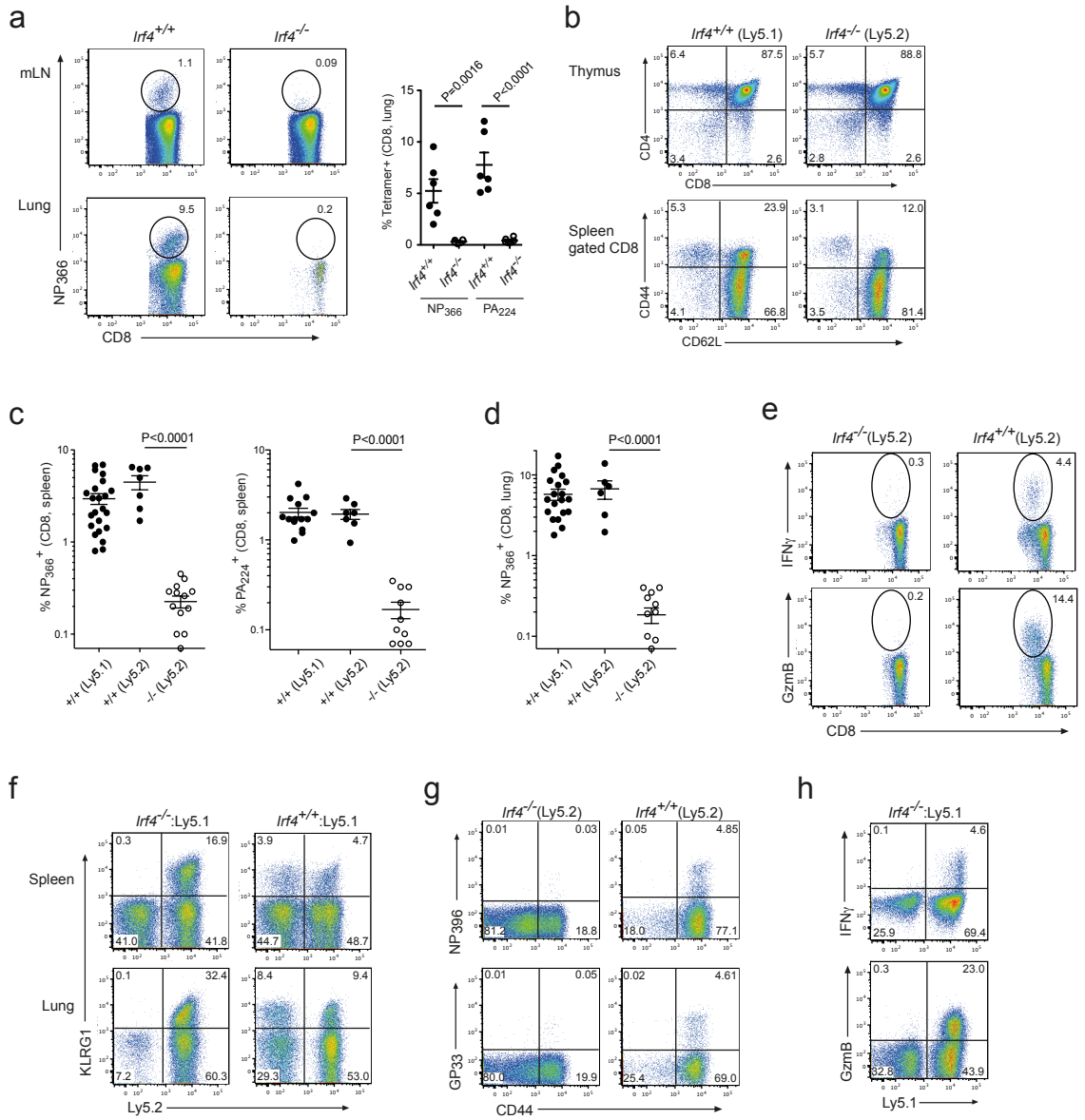

Supplementary Fig. 1. Intrinsic requirement for IRF4 for a productive CD8$^+$ T cell response. a. *Irf4*$^{+/+}$ or *Irf4*$^{-/-}$ mice were infected with influenza virus (HKx31). 10 days later CD8$^+$ T cells in the organs as indicated were analysed by flow cytometry for the presence of antigen-specific cells by tetramer staining. **b-h.** Mixed bone marrow chimeric mice generated by reconstituting Ly5.1 mice with *Irf4*$^{+/+}$ or *Irf4*$^{-/-}$ bone marrow (both Ly5.2) mixed with Ly5.1 bone marrow as indicated. **b.** Six weeks later CD8$^+$ T cells were analysed by flow cytometry in organs as indicated. **c-f.** Chimeric mice were infected with influenza virus (HKx31) six weeks after priming with a heterologous influenza virus (PR8). **c-d.** Frequencies of antigen-specific CD8$^+$ T cells determined by tetramer staining and flow cytometry in gated CD8$^+$ T cells as indicated. **e.** CD8$^+$ T cells as in (c) restimulated with NP_{366} peptide for 5 h and analysed for effector molecule expression as indicated by flow cytometry. **f.** CD8$^+$ T cells from influenza infected chimeric mice analysed by flow cytometry in organs as indicated. **g-h.** Chimeric mice were infected with Lymphocytic choriomeningitis virus (LCMV, WE). **g.** Frequencies of antigen-specific CD8$^+$ T cells determined by tetramer staining and flow cytometry as indicated. **h.** CD8$^+$ T cells from chimeric mice infected with LCMV restimulated with GP_{33} peptide and analysed by intracellular staining and flow cytometry for expression of effector molecules as indicated. Graphs show mean frequencies ±S.E.M.

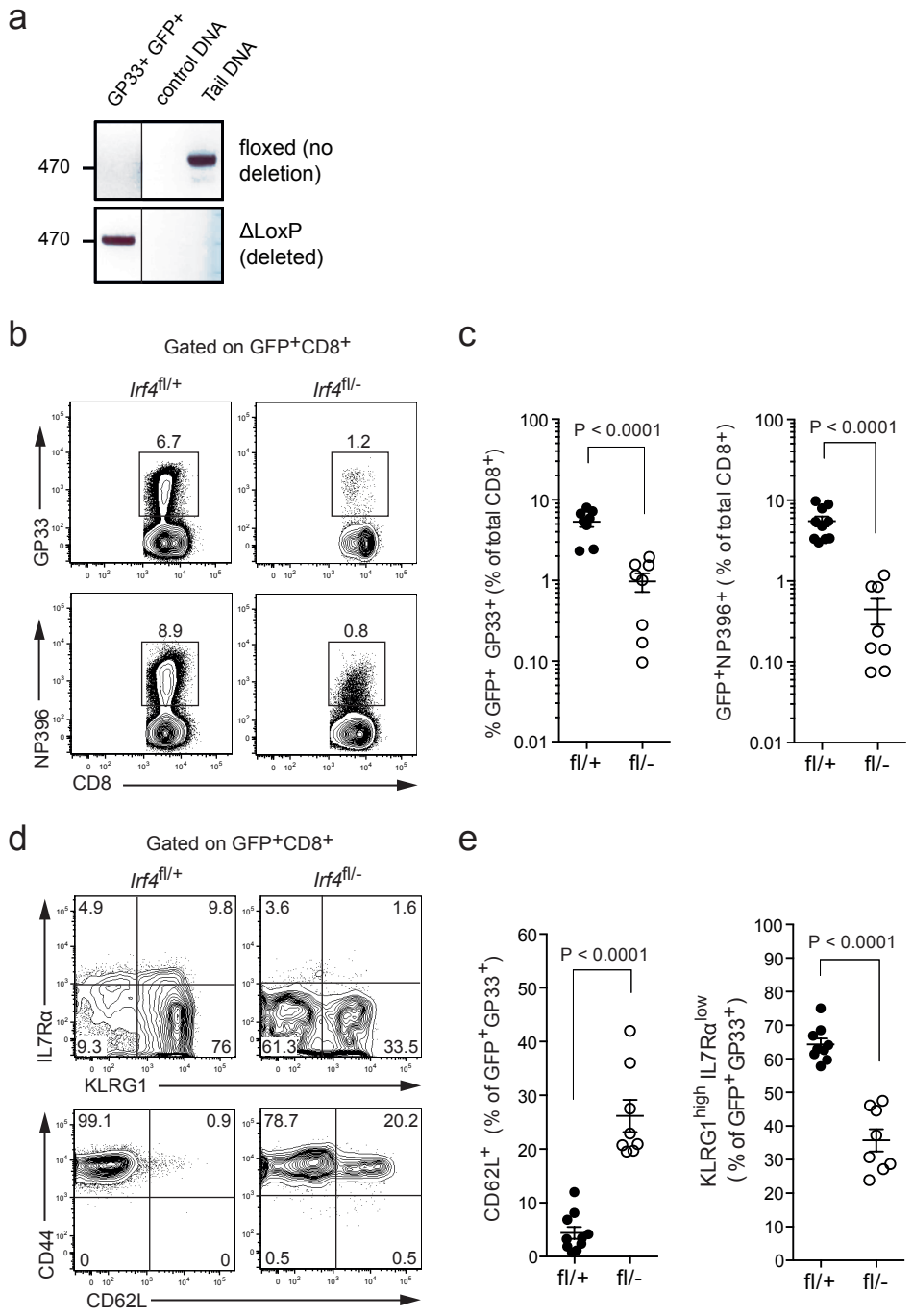

Supplementary Fig. 2. Conditional deletion of *Irf4* cripples antigen-specific CD8⁺ T cell responses during acute LCMV infection. Mice carrying floxed *Irf4* alleles were crossed to a transgenic mouse strain expressing Cre recombinase under the control of *granzyme B* gene regulatory elements and infected with LCMV. Deletion of the *Irf4* allele occurs after T cell activation, and is marked by expression of green fluorescent protein (GFP). **a.** Genomic PCR confirms the presence of the floxed allele in tail DNA and its deletion in sorted GFP⁺ CD8⁺ T cells specific for the LCMV epitope GP_{33}. **b-e.** Frequencies (b-c) and phenotype (d-e) of antigen-specific CD8⁺ T cells were measured by tetramer detection of cells specific for the LCMV epitopes GP_{33} or NP_{396} and staining with antibodies specific for the surface markers as indicated at day 9 post infection. Flow cytometry plots are representative and graphs are a summary of three independent experiments containing 2-3 mice each per group.

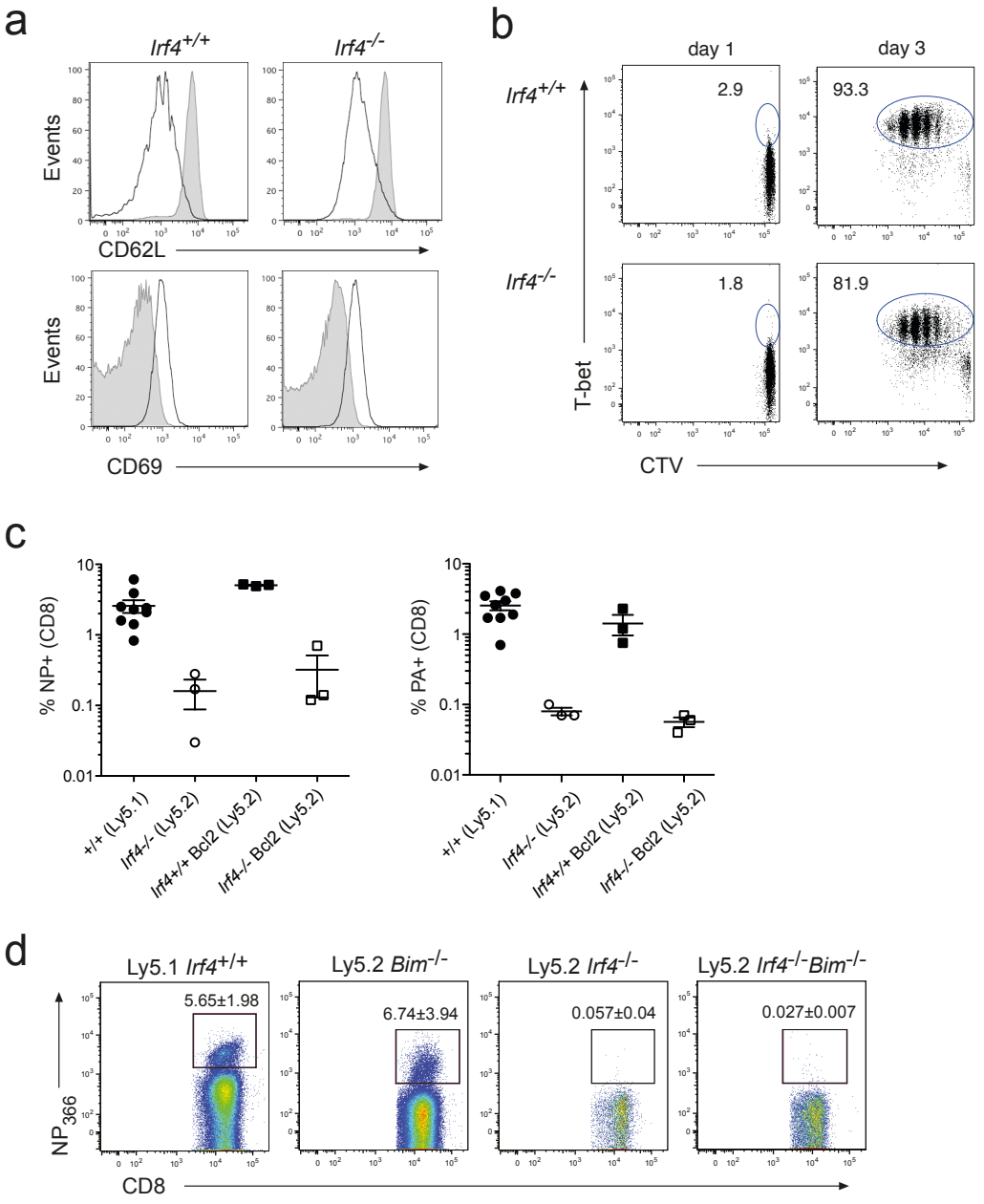

Supplementary Fig. 3. IRF4 is dispensable for activation, proliferation and effector molecule expression *in vitro*, and blockade of the intrinsic death pathway does not rescue antigen-specific IRF4-deficient CD8$^+$ T cells *in vivo*. a-b. CD44$^-$CD62L$^+$ naïve CD8$^+$ T cells of the indicated genotypes were flow-sorted, labelled with cell division tracker dye CTV and cultured in the presence of anti-CD3, anti-CD28 and IL-2. **a.** Expression of activation markers after 40 h in culture. **b.** Cell division profile as measured by CTV. Data are representative of 3 independent experiments. **c-d.** *Irf4*$^{+/+}$ or *Irf4*$^{-/-}$ bone marrow on a Vav-Bcl2 transgenic (c), Bim-deficient (d) or wildtype background as indicated were used to generate congenically marked mixed bone marrow chimeras in irradiated Ly5.1 recipient mice. After reconstitution mice were infected with influenza virus (HKx31). 10 days later splenocytes were stained with tetrameric complexes to identify antigen-specific CD8$^+$ T cells as indicated. Data in (c) are combined from three individual mice; horizontal line shows the mean ±S.E.M.; data in (d) are representative of 6 individual mice.

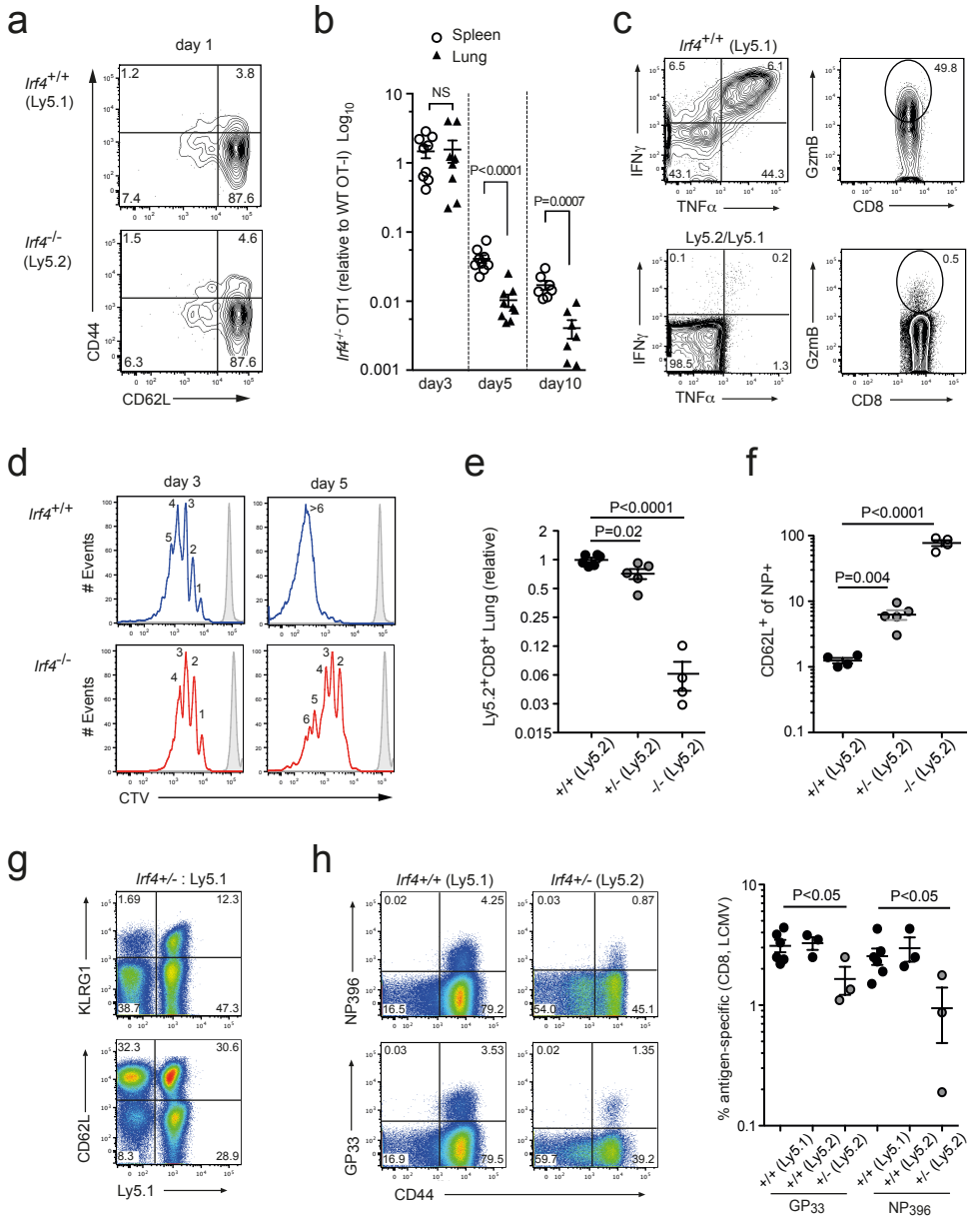

Supplementary Fig. 4. IRF4 is required for a productive CD8⁺ T cell response in a dose dependent manner. a-d. Each 2.5x10^5 OT-I CD8$^+$ T cells of indicated genotypes were transferred into F1 recipients (Ly5.1 x Ly5.2), which were infected with influenza virus expressing ovalbumin (HKx31-OVA) 1 day prior to cell transfer. **a.** Flow cytometric analysis of donor OT-I T cells in the lung-draining mediastinal lymph node 1 day after transfer. **b.** Ratio of *Irf4*$^{+/+}$ and *Irf4*$^{-/-}$ OT-I T cells at indicated times after transfer. NS - not significant. **c.** Flow cytometric analysis of restimulated donor-derived *Irf4*$^{+/+}$ OT-I T cells (upper panel) and endogenous CD8$^+$ T cells (lower panel) in the spleens 10 days after transfer. **d.** Division profiles measured by CTV dilution of donor OT-I T cells in HKx31-OVA infected mice at indicated times. Numbers indicate corresponding individual divisions. Shaded - freshly CTV stained cells. **e-h.** Chimeric mice generated from *Irf4*$^{+/+}$, *Irf4*$^{+/-}$ or *Irf4*$^{-/-}$ (all Ly5.2) bone marrow mixed with Ly5.1 bone marrow as indicated were infected with influenza virus (HKx31) (**e, f**) or LCMV (**g, h**). Relative contribution (**e**) or expression of CD62L (**f**) on NP$_{366}$-specific CD8$^+$ T cells in influenza-infected mice. Frequencies of effector cells measured by KLRG1 staining (**g**), and LCMV specific cells by tetramer detection of CD8$^+$ T cells (**h**).

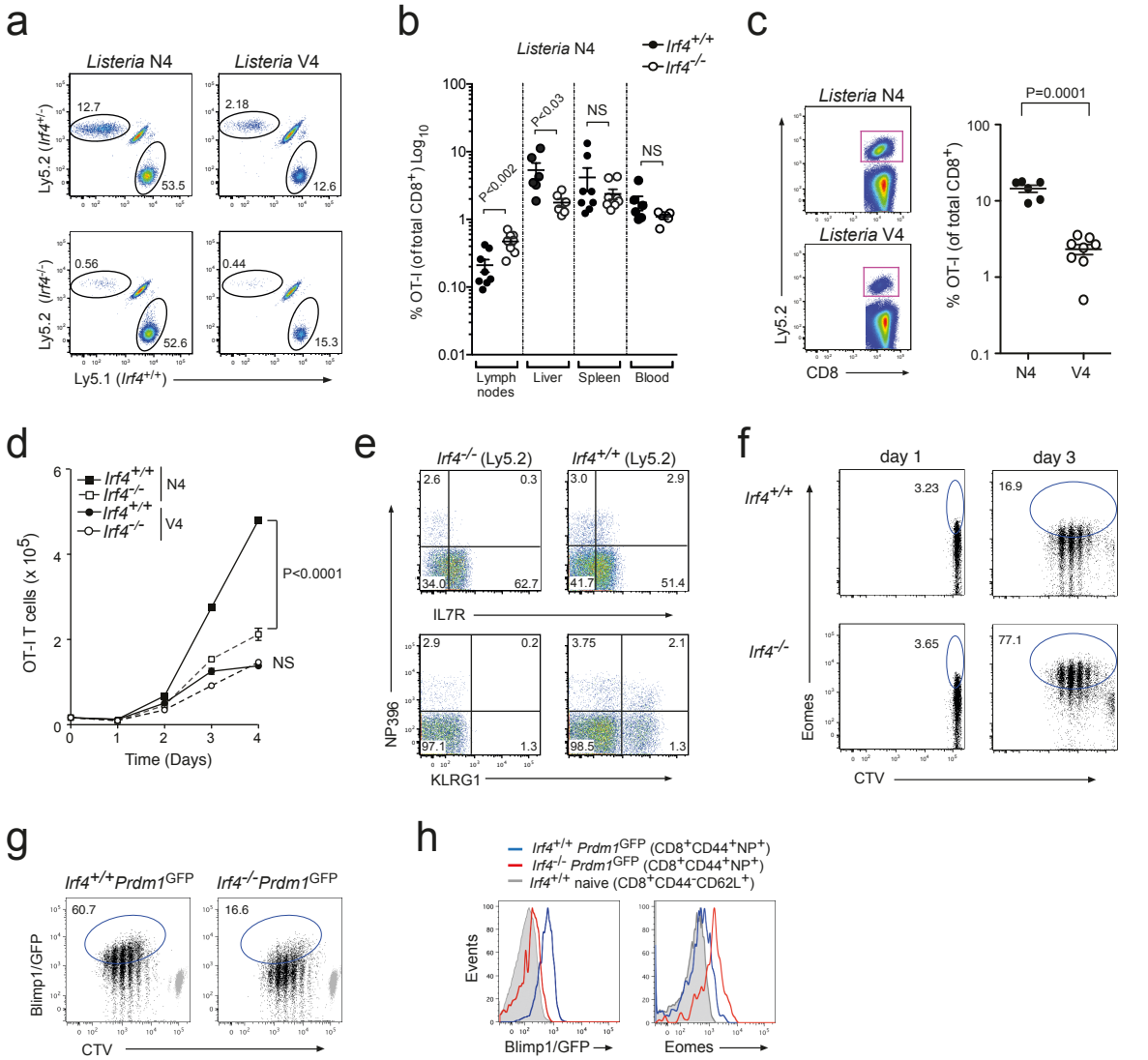

Supplementary Fig. 5. Impaired expansion and differential expression of selected molecules in IRF4-deficient CD8⁺ T cells. a-b. Each 1x10^5 OT-I T cells of the indicated genotypes were transferred into F1 mice (Ly5.1 x Ly5.2), which were infected with *Listeria* N4 (Lm-N4) or V4 (Lm-V4). Frequencies of OT-I T cells 3 days post infection. NS - not significant. **c.** 1x10^5 *Irf4*$^{+/+}$ OT-I CD8⁺ T cells were adoptively transferred into congenically marked recipient mice, infected with *Listeria* N4 (Lm-N4) or V4 (Lm-V4). Graph shows proportion of donor T cells in comparison to endogenous CD8⁺ T cells in spleen 5 days post infection. **d.** 2x10^4 OT-I T cells of the indicated genotypes were stimulated *in vitro* in the presence of N4 or V4 OVA peptide and IL-2. Cell numbers were determined at the times indicated after the start of culture. **e.** Mixed bone marrow chimeric mice as in Suppl. Fig. 1 were infected with LCMV. Ly5.2⁺CD8⁺ T cells in the lymph nodes were analysed by flow cytometry for expression of IL-7R and KLRG1 on antigen specific cells. **f-g.** Naïve CD8⁺ T cells of the indicated genotypes were labelled with cell division tracker dye CTV, cultured with CD3 and CD28 antibodies, IL-2 and IL-12, and analysed at times as indicated by intracellular staining (f). Blimp1 expression as measured using a *Prdm1*^{gfp} reporter allele (g). **h.** *Prdm1*-GFP and Eomes expression in antigen-specific (NP_{366}) CD8⁺ T cells in the lymph nodes of influenza infected bone marrow chimeric mice gated as indicated.

a

ID	Associated Network Functions	Score
1	Carbohydrate Metabolism, Molecular Transport, Small Molecule Biochemistry	37
2	Cell Morphology, Hematological System Development and Function, Cell Cycle	36
3	Nucleic Acid Metabolism, Small Molecule Biochemistry, Amino Acid Metabolism	36
4	Dermatological Diseases and Conditions, Developmental Disorder, Hereditary Disorder	36
5	RNA Post-Transcriptional Modification, DNA Replication, Recombination, and Repair, Gene Expression	36

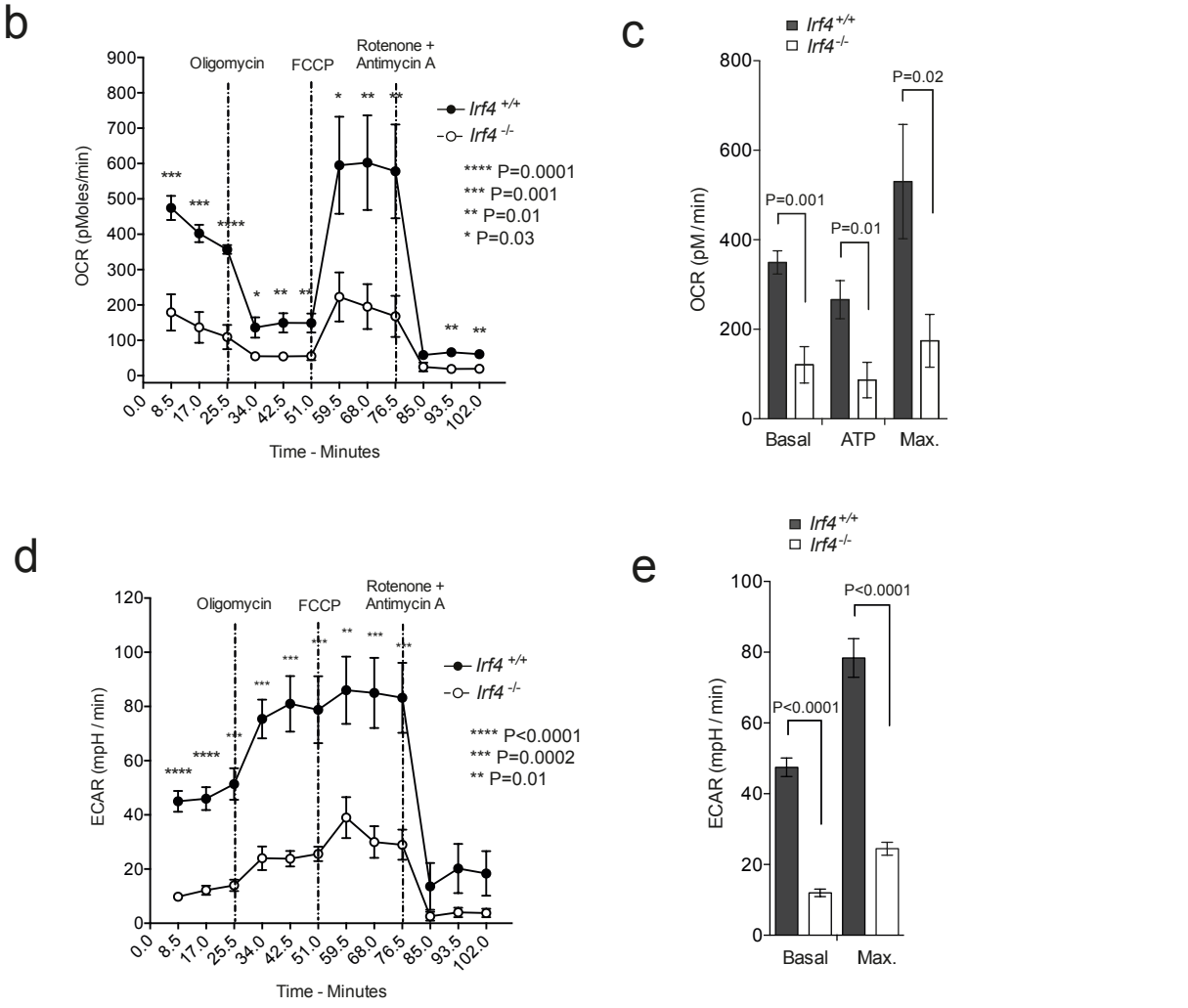

Supplementary Fig. 6. Impaired metabolic function of IRF4-deficient CD8⁺ T cells *in vitro*. a. The five top scoring networks identified by Ingenuity Pathway Analysis (IPA) of genes differentially expressed between *Irf4*$^{-/-}$ and *Irf4*$^{+/+}$ OT-I T cells stimulated with N4 OVA peptide as in Fig. 5. The dataset was used to run a Core analysis based on Ingenuity Knowledge Base, which included direct and indirect interactions based upon experimentally observed data curated from published literature sources. **b-e.** Extracellular flux analysis of in vitro activated (48 h) CD8⁺ T cells of the indicated genotypes. Oxygen consumption rate (OCR, **b-c**). Extracellular acidification rates (ECAR, **d-e**). Data are the mean ±S.E.M. from 3 biologically independent experiments.

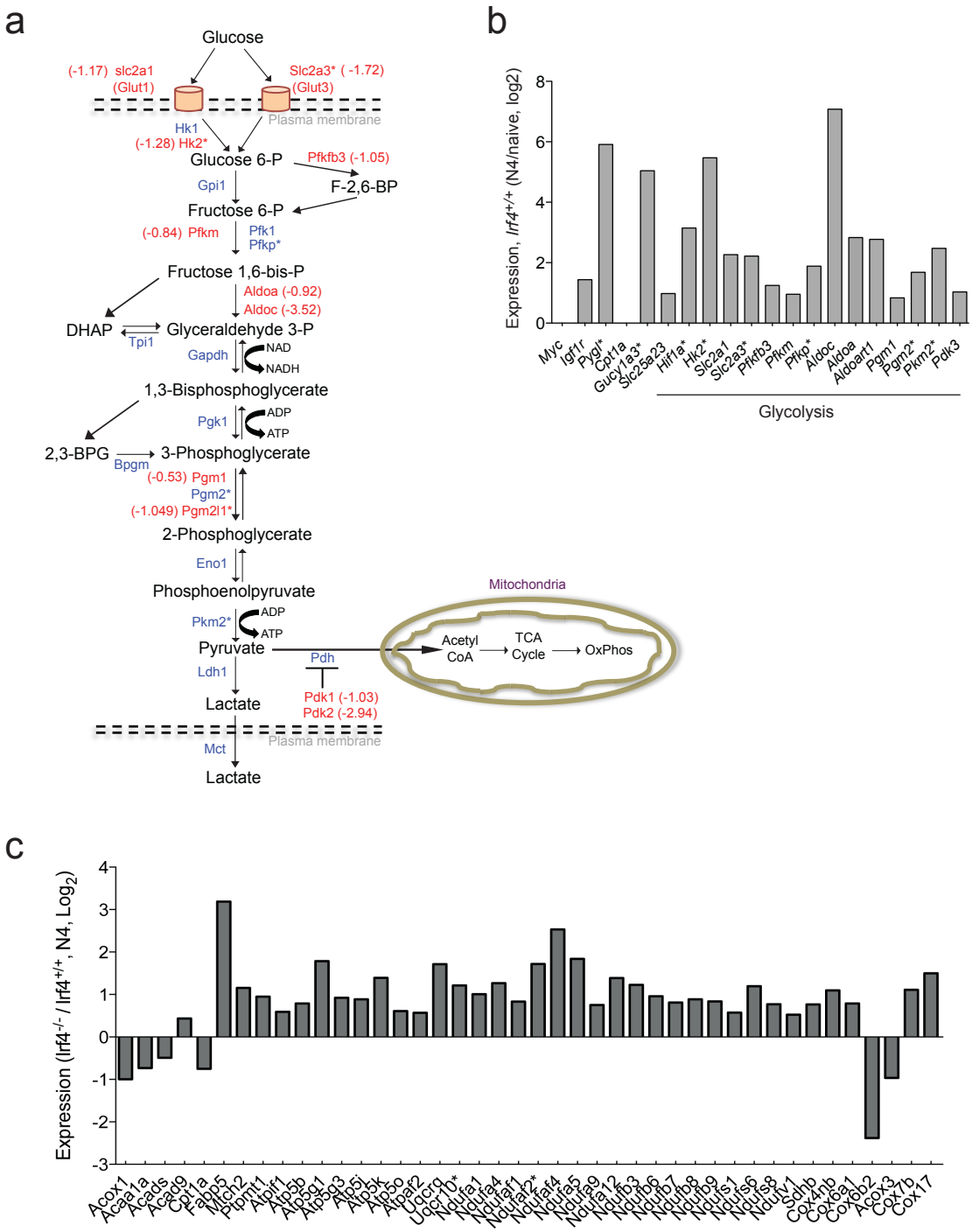

Supplementary Fig. 7. IRF4 and T cell activation regulate genes involved in glycolysis. a. Model of cellular glycolysis, adapted from Wang et al. (2011). Genes differentially expressed between wildtype and IRF4-deficient cells stimulated with N4 peptide are shown in red with log2 fold changes in brackets. Genes marked with * show binding of IRF4 as found in ChIP sequencing analysis. Numbers indicate log2 fold changes as determined by RNA sequencing. **b.** Changes in expression levels of genes involved in glycolysis after activation of wildtype $CD8^+$ T cells. **c.** Transcript levels of differentially expressed genes related to OXPHOS in OT-I T cells. Data in b, c were determined by RNA-sequencing and are the ratio of FPKM values (log2).

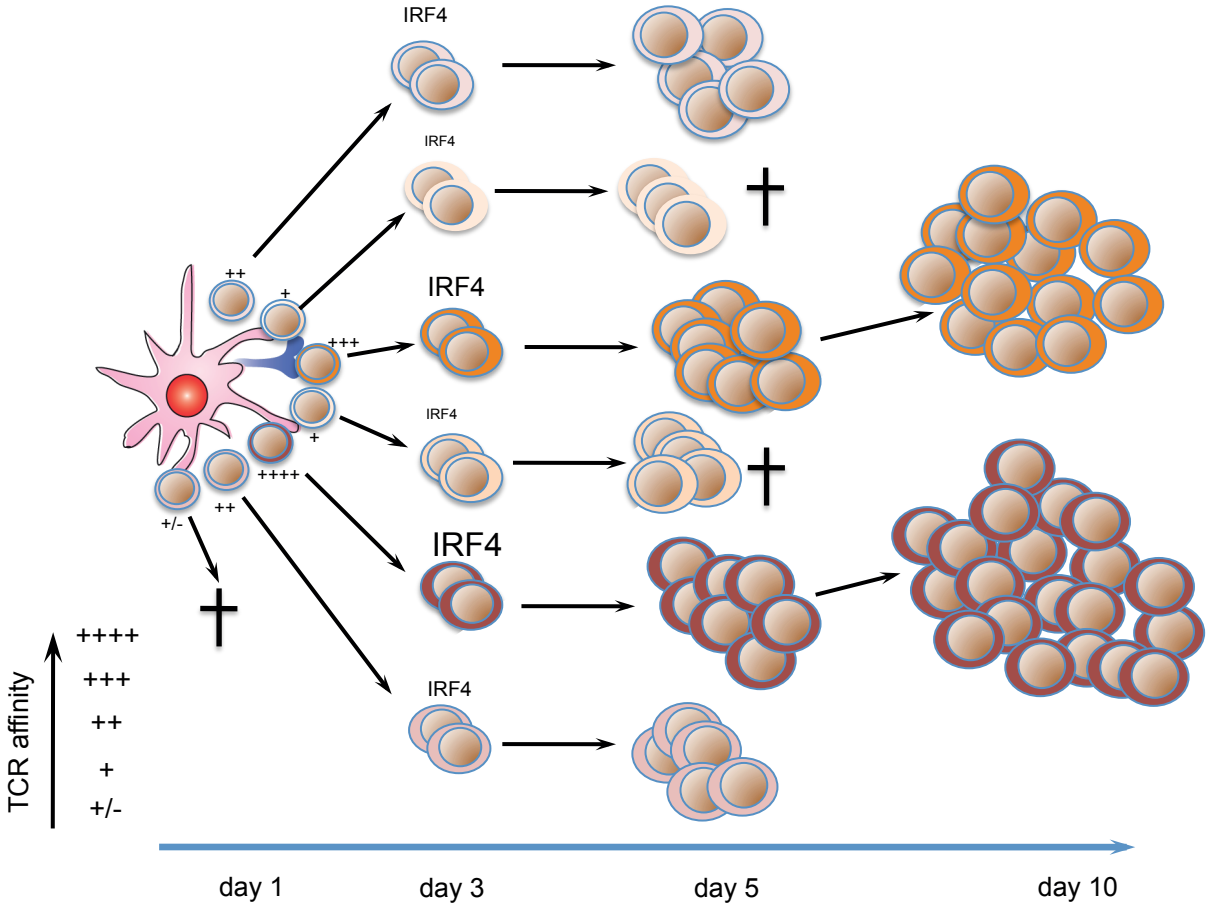

Supplementary Fig. 8. Model of clonal competition in CD8⁺ T cells based on affinity-driven IRF4 expression. CD8⁺ T cell clonotypes bearing TCR's of different affinity to the MHCI/peptide complexes presented by antigen presenting cells (left). Clonotypes with sufficiently high affinity undergo proliferation and dependent on the affinity of the TCR-MHCI/peptide interaction express different amounts of IRF4 (middle). Dependent on the amounts of IRF4 expressed cells undergo extensive clonal expansion during which clones of lower affinity that show lower expression of IRF4 will be outcompeted by high-affinity clones that express high levels of IRF4. The result is a dominance of a limited number of high-affinity clones at the peak of the CD8⁺ T cell response (right). Low affinity clones will die during the course of the response or contribute to memory T cell development. Different amounts of IRF4 are depicted by different font size; different TCR affinity by different numbers of '+'; horizontal arrow represents progression through the T cell response in time (days).

Supplementary Tabe 1. The 200 genes most differentially expressed between OT-1 CD8 T cells stimulated with low affinity (V4) and high affinity (N4) OVA peptide (V4 vs N4), as depicted in Figure 5a.

EntrezID	Symbol	logFC	P.Value	FDR
14938	Gzma	6.303397688	0.000387497	0.014646373
12772	Ccr2	6.27860463	0.001037099	0.022668493
60596	Gucy1a3	-5.912018103	7.43E-07	0.00068368
13813	Eomes	5.876521094	5.35E-09	7.48E-05
66141	Ifitm3	5.022407535	5.08E-05	0.006397696
29817	Igfbp7	-4.660992453	3.65E-05	0.00555657
71884	Chit1	-4.488960472	1.12E-05	0.002897233
16904	Gzmm	4.379853355	2.41E-07	0.00068368
12774	Ccr5	4.338609682	0.000249758	0.01291988
68404	Nrn1	-4.261218281	2.35E-06	0.001170476
59310	Myl10	4.245099622	0.003528634	0.040287313
75429	Fam183b	-4.241591064	0.0002517	0.012972308
140795	P2ry14	4.10974265	8.53E-07	0.00068368
20341	Selenbp1	-4.034708933	2.31E-06	0.001170476
18186	Nrp1	-3.987419438	4.98E-06	0.001657621
94214	Spock2	-3.901022356	1.51E-06	0.001050485
14728	Lilrb4	3.821176131	0.002263448	0.032309185
16001	Igf1r	-3.763282974	5.27E-07	0.00068368
381738	Ccdc164	3.754054903	0.001474755	0.026879628
320407	Klri2	-3.719358014	9.68E-06	0.002600115
14945	Gzmk	3.629954199	3.52E-08	0.000245481
12709	Ckb	-3.585864304	2.13E-05	0.004012
12182	Bst1	-3.468499806	0.000592493	0.017607138
17179	Matk	-3.390488947	4.93E-07	0.00068368
11486	Ada	3.3238499	0.000120566	0.009926946
56188	Fxyd1	-3.288455652	0.002732016	0.035369844
326620	Hist1h4b	3.256811297	4.84E-05	0.006263409
68713	Ifitm1	3.150986684	0.002154613	0.031584612
17470	Cd200	-3.121868097	5.72E-05	0.006771551
18566	Pdcd1	-3.094947805	5.39E-07	0.00068368
57780	Fxyd7	-3.014642609	5.30E-05	0.006513875
14103	Fasl	2.998127004	0.004013155	0.043116716
22163	Tnfrsf4	-2.955643739	0.00331638	0.038847944
110095	Pygl	-2.907829167	2.50E-06	0.001202934
22339	Vegfa	-2.8628964	0.006227503	0.05378585
102502	Pls1	-2.730161154	8.81E-07	0.00068368
12305	Ddr1	-2.705159924	5.47E-06	0.001736298
56075	Pdss1	2.684779801	0.000689687	0.018590815
16401	Itga4	-2.676188888	4.34E-07	0.00068368
103140	Gstt3	-2.649284516	6.29E-05	0.007031941
171543	Bmf	-2.641380223	6.84E-05	0.007294582

66395	Ahnak	-2.589762847	5.00E-05	0.006342425
14065	F2rl3	2.552500577	0.000142679	0.010219466
12520	Cd81	-2.543638114	4.89E-06	0.001657621
72500	Ier5l	-2.539841387	1.80E-05	0.003605982
16592	Fabp5	2.518636501	0.001745177	0.02865189
77590	Chst15	-2.481291824	7.35E-05	0.007362796
227753	Gsn	-2.446779186	0.000171183	0.010798764
16656	Hivep3	-2.441783724	0.003645015	0.040857783
211770	Trib1	-2.436347936	4.95E-05	0.006342425
238393	Serpina3f	2.430805844	0.001733888	0.028591751
333182	Cox6b2	-2.420894813	0.001430925	0.02656653
100113364	Snora15	2.372320987	0.000510202	0.016361386
20810	Srm	2.356859257	0.000390808	0.014646373
57908	Zfp318	-2.351270554	8.75E-07	0.00068368
14200	Fhl2	2.327275236	5.56E-05	0.006703648
18102	Nme1	2.323029436	5.98E-07	0.00068368
68194	Ndufb4	2.304015392	0.002910593	0.036282437
110454	Ly6a	2.280249974	8.21E-08	0.000382248
22779	Ikzf2	-2.245750533	0.000260386	0.013264285
80720	Pbx4	-2.24467724	0.000185386	0.011160724
11676	Aldoc	-2.244362545	0.000130839	0.010219466
11881	Arsb	2.241109376	7.19E-06	0.002091461
625929	Rps19-ps4	2.227926369	0.001632377	0.027894606
70747	Tspan2	-2.210708681	4.92E-06	0.001657621
17969	Ncf1	-2.208109067	4.74E-06	0.001657621
319148	Hist1h3c	2.207456058	0.000617582	0.018083376
52377	Rcn3	-2.202402824	0.000133717	0.010219466
54135	Lsr	-2.198883295	0.001258672	0.025171812
252838	Tox	-2.188971584	1.18E-05	0.002958178
68133	Gcsh	2.188471126	0.000546108	0.016850987
237887	Slfn10-ps	-2.1672946	0.00039197	0.014646373
56742	Psrc1	-2.159863061	0.003822674	0.041875516
11565	Adssl1	-2.155282126	0.000167937	0.010766464
319183	Hist1h2bj	2.149291311	0.000298376	0.013753832
66083	Setd6	2.134697941	0.000328908	0.013775644
13849	Ephx1	-2.128153611	0.000118863	0.009926946
380684	Nefh	2.125906726	0.00461717	0.046251291
170755	Sgk3	2.112339426	7.53E-06	0.002127227
16197	Il7r	-2.099856753	0.004857407	0.047343617
329739	Fam102b	-2.097302637	2.21E-06	0.001170476
16768	Lag3	-2.091040991	4.22E-05	0.00574222
50997	Mpp2	-2.08730208	4.51E-05	0.006052004
66972	Slc25a23	-2.0628188	5.17E-06	0.001680382
16988	Lst1	-2.045841197	0.000680317	0.018486353
226122	Ubtd1	2.02044001	0.000702283	0.018826851
228765	Sdcbp2	-2.016644136	0.0083804	0.064066256

319156	Hist1h4d	2.014677381	0.004666188	0.046452355
21452	Tcn2	-2.004277948	0.000644622	0.018188759
67895	Ppa1	1.986908888	1.47E-05	0.003251578
12703	Socs1	1.963095324	2.52E-05	0.004399887
21858	Timp2	-1.961313608	1.42E-05	0.003221772
15368	Hmox1	1.959960523	0.004898675	0.047517573
69202	Ptms	-1.957092003	5.70E-05	0.006771551
21929	Tnfaip3	-1.951773568	0.000295818	0.013753832
12850	Coq7	1.940038819	0.000234542	0.012502205
14939	Gzmb	1.932043906	0.002944394	0.03639323
68151	Wls	-1.917909057	0.000478346	0.016021715
18483	Palm	-1.916571688	0.00069026	0.018590815
216156	Wdr18	1.902499407	0.000138749	0.010219466
18392	Orc1	1.893719658	0.001989303	0.030266445
72400	Pinx1	1.889246126	0.003681996	0.041042644
23992	Prkra	-1.87699197	0.001702755	0.028417619
211401	Mtss1	-1.868912477	7.88E-05	0.007751685
78653	Bola3	1.864019668	0.002628394	0.034502609
22042	Tfrc	1.856716904	0.000746616	0.019387961
17299	Mettl1	1.842620761	0.007270201	0.058697345
73690	Glipr1	1.832360748	0.000699718	0.018794167
19280	Ptprs	-1.828384228	3.14E-05	0.005099602
67242	Gemin6	1.826764204	0.001123167	0.023718768
22171	Tyms	1.824228817	3.72E-05	0.00555657
654824	Ankrd37	-1.82273858	0.000779454	0.019641193
76199	Med13l	-1.80862296	0.000224188	0.012183811
232943	Klc3	-1.800166348	1.75E-05	0.003605982
72313	Fryl	-1.79919178	2.31E-05	0.004186077
109689	Arrb1	-1.798941975	0.001408933	0.026347435
17977	Ncoa1	-1.797628795	2.86E-05	0.004753988
110172	Slc35b1	1.792223599	0.000123395	0.009962219
19385	Ranbp1	1.790772637	0.000164896	0.010766464
16194	Il6ra	-1.785912878	0.000447659	0.015553361
64657	Mrps10	1.785597814	0.00114148	0.023933216
69745	Pold4	-1.783226002	0.000457146	0.015804362
11658	Alcam	-1.781401268	1.43E-05	0.003221772
22145	Tuba4a	1.778781027	0.001432767	0.02656653
22288	Utrn	-1.77506366	6.99E-05	0.007362796
66491	Polr2l	1.771042551	0.002142722	0.03148832
66249	Pno1	1.767367307	0.000156954	0.010488874
23959	Nt5e	-1.765297148	0.003879652	0.04222426
16764	Aff3	-1.757360602	0.000943294	0.021669395
75605	Kdm5b	-1.754179768	0.000386856	0.014646373
18673	Phb	1.751532661	0.000759569	0.019554396
18618	Pemt	1.748882132	0.008880082	0.066150716
18477	Prdx1	1.743129558	0.000472601	0.016006644

20425	Shmt1	1.73991964	0.002365656	0.032975168
64011	Nrgn	-1.738021109	0.001939574	0.029900693
209378	Itih5	-1.734035332	4.23E-05	0.00574222
15983	Ifrd2	1.732176245	0.003083508	0.037667133
228730	Plk1s1	-1.718183698	0.000487059	0.016132083
52065	Mfhas1	-1.712980678	0.000510744	0.016361386
20527	Slc2a3	-1.711902035	0.006966487	0.057608596
108960	Irak2	-1.70594745	0.003345177	0.039032656
13170	Dbp	-1.705897103	3.62E-05	0.00555657
381290	Atp2b4	-1.702025638	0.000322798	0.013775644
69902	Mrto4	1.694093327	0.001170202	0.024285609
286940	Flnb	-1.693044996	0.000284956	0.013477762
69890	Zfp219	-1.691394843	0.000297566	0.013753832
83490	Pik3ap1	-1.680545547	0.002566315	0.034202022
30058	Timm8a1	1.673734057	0.001906785	0.029659615
66230	Mrps28	1.66943274	0.000664153	0.018342093
20649	Sntb1	-1.669086852	0.005572806	0.050853863
26922	Mecr	1.662273305	0.000476747	0.016006644
20539	Slc7a5	1.650562436	0.006995786	0.057646106
74104	Abcb6	1.643985279	0.002739378	0.035391788
276770	Eif5a	1.64137848	0.000774525	0.019641193
51793	Ddah2	-1.63639501	0.000421193	0.014997932
65960	Twsg1	-1.635228221	0.000555917	0.017027384
66973	Mrps18b	1.630805068	0.001820172	0.029212098
11951	Atp5g1	1.630459418	0.000315054	0.013775644
16439	Itpr2	-1.629364421	1.68E-05	0.003547965
14453	Gas2	-1.628163157	0.000117663	0.009926946
338523	Jhdm1d	-1.621597226	1.81E-05	0.003605982
77862	Thyn1	1.614454498	0.000423495	0.014997932
53600	Timm23	1.611443242	0.000639857	0.018188759
69928	Apitd1	1.611188576	0.005597931	0.050910511
58801	Pmaip1	-1.608486309	0.001792538	0.029044529
105689	Mycbp2	-1.6061847	0.000121037	0.009926946
28126	Nop16	1.605376944	0.001092557	0.023308633
14062	F2r	1.597596208	1.72E-06	0.001050485
67880	Dcxr	-1.596605717	0.001831818	0.029212098
69573	Hilpda	-1.594296876	0.003665597	0.040947218
13877	Erh	1.592214688	0.000106624	0.0094254
80981	Arl4d	-1.591804533	0.001292884	0.025290912
66257	Nicn1	-1.591316141	0.00047675	0.016006644
68278	Ddx39	1.585370117	2.79E-05	0.004751452
22256	Ung	1.584314584	0.000234516	0.012502205
18415	Hspa4l	-1.582880129	0.000317201	0.013775644
54369	Nme6	1.580797793	0.001902465	0.029655945
14190	Fgl2	1.579722737	3.49E-05	0.005544061
22223	Uchl1	1.572882434	0.001625279	0.027887304

108037	Shmt2	1.571561496	0.002276024	0.032404921
15064	Mr1	-1.568799044	0.000803506	0.019756643
17122	Mxd4	-1.567603234	0.00642489	0.05498556
327987	Med13	-1.560181142	2.21E-05	0.004062154
69071	Tmem97	1.559345655	0.001325123	0.025598885
18604	Pdk2	-1.554188899	0.007395111	0.059122788
237256	Zc3h12d	-1.548867664	3.85E-05	0.005608311
18263	Odc1	1.545023158	0.00034528	0.013947432
71375	Foxn3	-1.541182716	0.000111966	0.009713223
67239	Rpf2	1.54022574	0.000809426	0.019833787
20393	Sgk1	1.537384184	0.000138708	0.010219466
104444	Rexo2	1.536154001	3.77E-05	0.00555657
12514	Cd68	-1.535200665	0.004606912	0.046251291
17992	Ndufa4	1.533321648	0.005299814	0.049546524
17472	Gbp4	1.532854517	0.000326921	0.013775644
78749	Filip1l	-1.528977169	8.76E-05	0.008376202
66253	Aig1	-1.526415903	0.005205825	0.04902883
105638	Dph3	1.524999574	0.000263063	0.013264285
50784	Ppap2c	-1.524705054	0.00146762	0.026852509
101612	Grwd1	1.524654632	0.002622133	0.034469922
13025	Ctla2b	1.522855275	0.008781055	0.066001631

Supplementary Tabe 2. Mapping results of RNA and ChIP sequencing data.

Sample	Total number of reads	% mapped to mouse genome	% assigned to RefSeq genes (out of total # of reads)
Irf4$^{+/+}$_V4	12919854	99.5	78.4
Irf4$^{+/+}$_V4	12334822	99.4	76.5
Irf4$^{-/-}$_N4	12454324	99.3	75.5
Irf4$^{-/-}$_N4	18595382	99.4	76.1
Irf4$^{-/-}$_N4	19119234	99.4	75.9
Irf4$^{-/-}$_V4	13217130	99.3	69.7
Irf4$^{-/-}$_V4	13273338	99.5	76.3
Irf4$^{+/+}$_naive	19897364	99.1	74.3
Irf4$^{-/-}$_naive	18906594	97.8	72.9
IRF4-ChIP, CD8	25090966	87.7	
chromatin input	25820698	88.2	